

# A review of different modeling approaches used to simulate smoke transport and dispersion

Derek Mallia<sup>1</sup> and Adam Kochanski<sup>2</sup>

<sup>1</sup>University of Utah

<sup>2</sup>San Jose State University

November 24, 2022

## Abstract

A variety of smoke model frameworks are used to simulate smoke for research and forecast applications. Here, a comprehensive summary is provided which covers the many different smoke models that are available, while simultaneously highlighting some of the strengths and weaknesses of each model, along with the uncertainties surrounding each of these frameworks. This review also provides an in-depth discussion on coupled wildfire-atmosphere models, which is a relatively newer smoke modeling tool not previously discussed in other review papers. Key processes related to smoke transport and dispersion, such as the wildfire plume rise, are also discussed in length. This review wraps up with a discussion of future smoke modeling needs and potential new research directions for smoke transport and dispersion models.



AGU Books

## A review of different modeling approaches used to simulate smoke transport and dispersion

Journal:	<i>AGU Books</i>
Manuscript ID	2021-Jun-CH-1395.R2
Wiley - Manuscript type:	Chapter
Date Submitted by the Author:	28-Jan-2022
Complete List of Authors:	Mallia, Derek; University of Utah, Dept. of Atmospheric Sciences Kochanski , Adam; San Jose State University, Department of Meteorology and Climate Science
Primary Index Term:	3390 - Wildland fire model < 3300 - ATMOSPHERIC PROCESSES
Index Term 1:	305 - Aerosols and particles (0345 , 4801 , 4906) < 300 - ATMOSPHERIC COMPOSITION AND STRUCTURE
Index Term 2:	3307 - Boundary layer processes < 3300 - ATMOSPHERIC PROCESSES
Index Term 3:	345 - Pollution: urban and regional (0305 , 0478 , 4251) < 300 - ATMOSPHERIC COMPOSITION AND STRUCTURE
Index Term 4:	3365 - Subgrid-scale (SGS) parameterization < 3300 - ATMOSPHERIC PROCESSES
Keywords:	Smoke modeling, Wildland fires, Air quality, Aerosols, Numerical weather prediction, Coupled fire-atmosphere interactions
Abstract:	A variety of smoke model frameworks are used to simulate smoke for research and forecast applications. Here, a comprehensive summary is provided which covers the many different smoke models that are available, while simultaneously highlighting some of the strengths and weaknesses of each model, along with the uncertainties surrounding each of these frameworks. This review also provides an in-depth discussion on coupled wildfire-atmosphere models, which is a relatively newer smoke modeling tool not previously discussed in other review papers. Key processes related to smoke transport and dispersion, such as the wildfire plume rise, are also discussed in length. This review wraps up with a discussion of future smoke modeling needs and potential new research directions for smoke transport and dispersion models.



1 **Chapter 8: A review of modeling approaches used to simulate smoke**  
2 **transport and dispersion**

3 Derek V. Mallia<sup>1</sup> and Adam K. Kochanski<sup>2</sup>

4 <sup>1</sup>*Department of Atmospheric Sciences, University of Utah, Salt Lake City, UT*

5 <sup>2</sup>*Department of Meteorology and Climate Science, San José State University, San Jose, CA*

6 \*Corresponding author email: [Derek.Mallia@utah.edu](mailto:Derek.Mallia@utah.edu)

7 Version: January 28<sup>th</sup>, 2022; edits from NHF French, ed. on Jan 2<sup>nd</sup>, 2022.

8 **Book:** Fire, Smoke and Health: tracking the modeling chain from flames to health and wellbeing

9 **Running header:** Modeling smoke transport and dispersion

10

11 **Abstract:**

12 A variety of smoke model frameworks are used to simulate smoke for research and forecast

13 applications. Here, a comprehensive summary is provided which covers the many different

14 smoke models that are available, while simultaneously highlighting some of the strengths and

15 weaknesses of each model, along with the uncertainties surrounding each of these frameworks.

16 This review also provides an in-depth discussion on coupled wildfire-atmosphere models, which

17 is a relatively newer smoke modeling tool not previously discussed in other review papers. Key

18 processes related to smoke transport and dispersion, such as the wildfire plume rise, are also

19 discussed in length. This review wraps up with a discussion of future smoke modeling needs and

20 potential new research directions for smoke transport and dispersion models.

21

22

23

## 24 **1. Introduction**

25 Smoke is a product of the combustion process that contains various chemical species and  
26 particulates, which can degrade air quality across a broad range of spatiotemporal scales  
27 (Goodrick et al., 2012). Increased fire activity due to climate change (Westerling et al., 2006;  
28 Spracklen et al., 2009) and robust population growth across the western U.S. is expected to  
29 expose 82 million Americans to smoke in the coming decades (Liu et al., 2016a). As wildfires  
30 increase in frequency and intensity, it is imperative that tools are developed and improved upon  
31 for studying and forecasting smoke and combustion products detrimental to health, including  
32 particulate matter with a diameter less than 2.5  $\mu\text{m}$  ( $\text{PM}_{2.5}$ ) and precursors for ozone ( $\text{O}_3$ )  
33 formation downwind of the fire (Jaffe and Widger, 2012). Some objectives of smoke modeling  
34 includes limiting the public's exposure to unhealthy concentrations of smoke and determining  
35 how smoke could impact active fire management operations during active wildfires and  
36 prescribed burns (Kochanski et al., 2018; Peterson et al., 2020). Prescribed burns, for example,  
37 are used to manage forests, combat wildfires, and mitigate public exposure to smoke (Rappold et  
38 al., 2014). Igniting fires in a controlled setting, limits the intensity and fuel consumption of  
39 wildfires, and therefore reduces smoke production relative to uncontrolled wildfires with no fuel  
40 thinning (Haikerwal et al., 2015). Smoke models can also be used to forecast meteorology that  
41 can favorably disperse smoke from prescribed burns, and to inform burn decisions so that the  
42 public's exposure to unhealthy concentrations of smoke is limited (Lahm, 2015). Finally, smoke  
43 models are also needed to elucidate processes that govern the chemical makeup and transport of  
44 smoke. Such processes range from small-scale mechanisms that drive the wildfire plume rise  
45 (Mallia et al., 2020a) to the global impacts of smoke aerosols on climate (Peterson et al., 2018;  
46 Christian et al., 2019).

47 Forecasting and simulating smoke transport is an inherently difficult task as wildfires and  
48 smoke transport is a multi-scale phenomenon with many interconnected processes (Figure 1).  
49 For example, the wildfire plume rise, which is responsible for injecting smoke in the atmosphere,  
50 is controlled by many factors such as atmospheric stability, wind shear, heat fluxes, and fire  
51 geometry (Figure 1) (Freitas et al., 2007; 2010). Pyroconvective plumes can also affect local  
52 meteorology by increasing near surface winds (Clements et al., 2007; Kochanski et al., 2013),  
53 shading areas underneath the plume (Figure 1) from direct insolation (Robock, 1988; 1991;  
54 Lareau et al., 2015; Walters et al., 2016; Kochanski et al., 2019), and in rarer cases; plumes can  
55 initiate fire-generated thunderstorms (i.e pyrocumulonimbus; Fromm et al., 2010). These  
56 processes can often feedback to the local meteorology at the fire line and impact wildfire  
57 behavior.

58 The amount of smoke and heat that is being emitted by the fire serve as essential inputs for  
59 smoke models (see #1 in Figure 1). Smoke emissions are used to determine the mass flux of  
60 chemical species into the atmosphere while the heat flux and fire area are important variables for  
61 determining how far up smoke might be lofted into the atmosphere. However, accurately  
62 quantifying fire emissions and heat fluxes from wildfires remains challenging. Estimating smoke  
63 emissions and heat fluxes requires information on the exact location and geospatial context of  
64 active burning, a description of fuels that are being consumed by the fire, and how intensively  
65 that fuel burns (see Chapter 5). Previous work has estimated that uncertainties associated with  
66  $PM_{2.5}$  emissions from fires could be as high as 64% (Urbanski et al. 2011). Errors in emission  
67 estimates often stem from the errors in the estimated burned area, which can be difficult to  
68 quantify due to ambiguities associated with differentiating the burned from unburned areas  
69 within and around the fire perimeter (Battye and Battye, 2002). Emission factors for different

70 chemical species and aerosols emitted by the fire are yet another major source of uncertainty and  
71 can exhibit significant variability due to heterogeneous fuel type and condition (Urbanski, 2014),  
72 as well as combustion characteristics (flaming vs. smoldering) (Lobert, 1991; Yokelson et al.,  
73 1996; Chen et al., 2007; McKeeking et al., 2009; Burling et al., 2010). Lastly, burn severity,  
74 which is related to fuel consumption, can also affect emission estimates, and add uncertainties to  
75 smoke emission inventories (Urbanski et al., 2011).

76 Forecasting smoke emissions and heat fluxes adds additional challenges, as it requires a  
77 model to make future projections for fuel consumption, on top of the underlying assumptions  
78 needed to convert burned biomass into emissions of different chemical species and aerosol  
79 particles (see Chapter 7). The uncertainties surrounding fire-emitted fluxes can also influence the  
80 vertical plume extent and plume dynamics (Freitas et al., 2007), which in turn, can impact how  
81 smoke is transported and dispersed from the fire.

82 Many atmospheric and chemical modeling frameworks can be used to simulate the transport  
83 of smoke from wildfires and prescribed burns. These smoke modeling frameworks range from  
84 simple box and Gaussian plume models (Lavdas, 1996) to more sophisticated modeling systems  
85 that can simulate smoke on an atmospheric grid with full physics and photochemistry (Hu et al.,  
86 2008; Liu et. al, 2009; Hodzic et al., 2007; Grell et al., 2011, Larkin et al., 2009; Kochanski et  
87 al., 2016). The primary difference between smoke models is how they account for physical  
88 processes that govern smoke transport and dispersion (Figure 1), along with other underlying  
89 processes such as fire emissions and burn area, fire-atmosphere interactions, plume entrainment,  
90 atmospheric chemistry, aerosol physics and particle deposition, and plume entrainment (Figure  
91 1; Table 1). These models can also differ in terms of the reference frame that they use to  
92 simulation smoke, i.e., the Eulerian versus the Lagrangian perspective.

93 The type of model used to simulate smoke often depends on the application and the scientific  
94 question or application that the researcher or fire manager is addressing. For example, for some  
95 applications, a Gaussian plume models could be more practical for a case where the wind field is  
96 unidirectional and constant between the smoke source and receptor. However, if the user  
97 attempts to model a case where there is a large wildfire in complex terrain, with erratic wind  
98 fields generating intense pyro-convection, a Gaussian plume model may not be sufficient; thus,  
99 necessitating the need for a more complex and computationally demanding modeling framework  
100 such as a coupled fire-atmosphere model.

101 In the following sections of this Chapter (Section 2 & 3), we will provide a brief overview of  
102 important smoke-related processes (Section 2) while highlighting the different modeling  
103 frameworks used to simulate smoke transport (Section 3). Section 3 will be divided by smoke  
104 transport model type. This section will then be followed up with a list of plume-rise models,  
105 which are often integrated within various smoke transport models to vertically distribute smoke  
106 emissions (Section 4). Finally, Section 5 will summarize some of the major discussion points of  
107 Sections 2, 3 and 4, while Section 6 will discuss future smoke modeling needs and directions.

108

## 109 **2. Smoke-related processes**

110 As discussed in the previous section, smoke models need to represent many critical fire and  
111 atmospheric processes such as (1) fire growth or burned area, (2) smoke emissions, (3) the  
112 buoyant rise plume rise driven by the fire, (4) mixing between smoke plume and the ambient air  
113 outside of it, often referred to as entrainment, (5) deposition processes, (6) downwind smoke  
114 dispersion, and (7) plume chemistry (Figure 1). It should be emphasized that these processes do  
115 not operate independently, and are sometimes dynamically linked together (Fromm et al., 2010;

116 Lareau and Clements, 2016; 2017; Kochanski et al., 2019; Mallia et al., 2020a). For example,  
117 heat fluxes generated by the fire can sometimes result in intense pyroconvection. If the smoke  
118 plume reaches a high enough altitude, water vapor will condense into liquid cloud water that can  
119 aid in the formation of pyrocumulus (pyroCu) or pyrocumulonimbus (pyroCb) clouds. There  
120 have been several documented cases of pyroCbs reaching altitudes of 15-km or more (Fromm et  
121 al., 2010; Peterson et al., 2018). The range of scales involved in the dynamics of fire-generated  
122 plumes is immense as it encompasses small scale processes driving combustion and heat release  
123 at a fire front, up through large-scale global weather patterns, which are responsible for driving  
124 long-range smoke transport. The processes discussed above are conceptualized in Figure 1.

125 Currently, most smoke modeling frameworks are developed to deal with smoke transport  
126 targeted at specific spatiotemporal scales. It should be emphasized that assumptions made within  
127 one model may not necessarily be valid for another model that deals with smoke transport at a  
128 different scale. Thus, there is no single model that encompasses the full range of scales needed to  
129 explicitly resolve smoke generation, plume rise and dispersion. This concept is conceptualized in  
130 Table 1, where individual smoke models have ‘niches’ in the continuum of spatial and temporal  
131 scales. Combustion resolving models such as Wildland-Urban Interface Fire Dynamics  
132 Simulator (WFDS; Mell et al., 2007) and FIRETEC (Linn and Cunningham, 2005) operate at  
133 smaller scales while, models such as Daysmoke (Achte-meier et al. 2011) or WRF-SFIRE/WRF-  
134 FIRE (Mandel et al. 2011; Coen et al. 2013) and others focus on simulating smoke at larger  
135 spatiotemporal scales, but at the expense of small-scale processes that need to be simplified as  
136 parameterizations. Chemical transport models such as GEOS-CHEM resolves the coarsest  
137 processes, but simulates smoke at the largest scale possible (global). Aside from spatiotemporal  
138 scales, smoke models can also be classified based on how they represent critical smoke-related

139 processes and the frame of reference used to simulate smoke.

140

### 141 *2.1 Fire burn area and emissions*

142 The fire burned area and emissions, which are related to fire activity, are critical inputs for  
143 most smoke models (see Chapters 3 and 5). Fire burned area emission can be represented in  
144 several different ways within smoke models. In many cases, models simply rely on external fire  
145 emission inventories such as GFED (Van der Werf et al., 2010), FINN (Weidenmeyer et al.,  
146 2009), or MFLEI (Urbanski, 2017) to provide historical estimates of smoke emissions and fire  
147 area. Some fire emission inventories, such as Missoula Fire Laboratory Emission Inventory  
148 (MFLEI), include emission uncertainty estimates using a Monte Carlo analysis (Urbanski et al.,  
149 2011). A more comprehensive list and description of fire emission inventories can be found in  
150 **Chapter 4**. Satellites are also playing increasing large role to estimate fire emissions and heat  
151 fluxes. Operational smoke forecast models, such as HRRR-Smoke (Amohdavi et al., 2017), use  
152 satellite fire radiative power (FRP) to estimate smoke emissions and heat fluxes, and then scale  
153 fire activity by an average fire diurnal cycle. A subset of smoke models, mainly, coupled fire-  
154 atmosphere models, can project future fire activity based on a fire spread parametrization that  
155 accounts for local meteorology, fuel types and characteristics, and terrain.

156 FIRETEC and WFDS employ a physics-based approach for estimating fire growth and the  
157 burned area. The physics-based approach utilizes models that explicitly represents combustion,  
158 heat transfer, aerodynamic drag, and turbulence. These models can predict fire growth, which  
159 can be used to estimate the burned area at any time, along with the amount of fuel consumed, and  
160 subsequently, smoke emissions. While physics-based models represent the most realistic way to  
161 simulate combustion processes and fire progression (where and when a fire moves), they

162 simplify smoke transport processes such that smoke is assumed to be a passive tracer; thus,  
163 ignore smoke chemical transformations and radiative impacts. Finally, explicitly resolving  
164 combustion requires very detailed information about fuels at high spatial resolutions (order of  
165 meters) and therefore are very computationally demanding. Ultimately, this limits the size of  
166 simulated fires to less than 100 acres for physics-based approaches (Liu et al., 2019).

167 An alternative method for estimating fire progression can be accomplished through  
168 empirical-based parameterizations. The most widely used fire progression parameterization is the  
169 Rothermel surface fire spread model (Rothermel, 1972), which was developed within the United  
170 States Forest Service (USFS) during the 1960 and 1970s. Unlike the physics-based approach, fire  
171 spread models, like the Rothermel model, estimate fire growth rates through a quasi-empirical  
172 equation that relates fire spread to variables such as fuel type and characteristics, terrain slope,  
173 and wind. Since fire spread parameterizations rely on simple algebraic formulas, they estimate  
174 fire growth rates at a more modest computational cost (Liu et al., 2019). Coupled fire-  
175 atmosphere models such as WRF-SFIRE and WRF-FIRE employ an empirical-based  
176 parameterization to estimate fire growth, fuel consumption, fire heat fluxes, and smoke  
177 emissions.

## 178 *2.2 Plume rise*

179 The fire plume rise, *i.e.*, *the vertical transport of smoke*, is yet another important  
180 phenomenon that must be accounted for when simulating smoke transport from prescribed burns  
181 or wildfires. The plume rise is primarily driven by heat released from the fire along with the  
182 atmosphere's response to this heating (Figure 1). Essentially, the fire plume rise acts as a  
183 chimney, which can loft smoke high in the atmosphere, with plume rise altitudes sometimes  
184 reaching upwards of 15-km in exceptional cases (Fromm et al., 2010; Peterson et al., 2018). The

185 height over which the plume extends is referred to as the plume injection height and is a function  
186 of intensity and geometry of surface fire, ambient atmospheric conditions such as stability, wind  
187 shear, and moisture profile, and plume microphysics.

188 The smoke injection height can control for the fate of smoke, among other factors, such a  
189 large-scale weather patterns and convection. For example, when smoke is lofted at a lower  
190 altitude, weaker winds near Earth's surface can limit how far the smoke is transported, while  
191 particle removal processes such as dry deposition are more dominant near the ground (Zhang et  
192 al., 2001; Emerson et al., 2020). For cases of limited smoke transport, smoke can accumulate in  
193 areas local relative to the smoke source region, which can further degrade the air quality, locally  
194 (Kochanski et al., 2019). Conversely, smoke that is injected higher in the atmosphere will often  
195 travel further from the fire and can degrade air quality over a much larger geographical region.  
196 At this same time, the fire plume rise can also cause the smoke to overshoot areas near the fire,  
197 therefore limiting local impacts of smoke on air quality.

198 The injection height can also play a vital role on aerosol feedbacks within the climate system.  
199 Smoke that is lofted into the upper troposphere and lower stratosphere can have a much longer  
200 residence time relative to smoke aerosols injected into the lower troposphere and planetary  
201 boundary layer (PBL). Previous research has demonstrated that smoke lofted further up in the  
202 atmosphere can have greater impacts on climate forcing (Barnes and Hofmann, 1997; Robock,  
203 2000). The few examples provided above exemplify the need to accurately resolve the fire plume  
204 rise for smoke modeling applications.

205 A variety of different modeling approaches currently exist for quantifying the vertical  
206 transport of smoke by fire plume rise (Liu et al., 2010; Paugnam et al., 2016). These models  
207 range from simple approximations that release smoke at altitudes that correspond climatological

208 averages to full-physics models that can explicitly resolve the wildfire plume rise and plume rise  
209 dynamics (Trentmann et al., 2006; Kochanski et al., 2016). Sometimes plume rise models are  
210 integrated directly within smoke transport models (Larkin et al., 2009; Amohdavi et al., 2017)  
211 while other frameworks run the plume rise model in an offline setting (Mallia et al., 2018). A  
212 separate section in this chapter (**Section 4**) has been dedicated to describing the various plume  
213 rise modeling approaches used within smoke transport models.

214 Work carried out by Mallia et al. (2018) found that simulations of local-scale smoke  
215 transport were highly sensitive to the altitude in which emissions were injected at. A regional-  
216 based study by Walters et al. (2016) also found that smoke transport within WRF-Chem was  
217 sensitive to the plume injection height, with simulated aerosol optical depth values varying by as  
218 much as  $\pm 50\%$  depending on the plume height injection scheme that was used. In both studies,  
219 the simulations that attempted to estimate vertical plume extent performed better than model  
220 configurations that injected smoke emissions at single level or at the surface.

221 While the work outlined above has indicated the plume rise models have improved smoke  
222 simulations, several studies have noted inconsistencies between simulated and observed plume  
223 top heights (Val Martin et al., 2012; Raffuse et al., 2012). Val Martin et al. (2012) concluded that  
224 implementing plume rise models within smoke transport models “remains a difficult  
225 proposition” given the uncertainties surrounding the formulations of plume rise  
226 parameterizations and model inputs such as fire heat fluxes and area.

### 227 *2.3 Meteorology*

228 Meteorological models are often needed to simulate the downwind transport of smoke.  
229 Numerical weather prediction models (NWP) are the most widely used method for characterizing  
230 the three-dimensional structure of meteorological variables such as winds, temperature,

231 humidity, and pressure. Approximated forms of partial differential equations that describe the  
232 atmosphere are used to predict the state of the atmosphere for any given time and location. These  
233 equations are solved numerically on an atmospheric mesh that covers the simulated domain  
234 (Kalnay, 2003). Certain meteorological processes, such as cloud microphysics, land-atmosphere  
235 interactions, and solar radiation are usually too small or too complex to be explicitly accounted  
236 for by governing equations. Thus, most NWP models parameterize these processes using a  
237 variety of different methods (Kalnay, 2003). Depending on the grid spacing of the  
238 meteorological model, certain processes can be either parametrized (if the model resolution is too  
239 coarse to resolve them) or explicitly resolved if the model resolution is sufficient (Weisman et al.  
240 2008; Shin et al. 2015). NWP models such as Weather Research and Forecast model (WRF;  
241 Powers et al., 2017) operate across a large range of spatiotemporal scales and therefore  
242 parameterize processes such as convection in coarser domains but can explicitly resolve  
243 convective processes when run at a fine spatial resolution.

244 In essence, NWP models provide the inputs needed to simulate the transport of smoke from  
245 the fire source to the area(s) of interest. Some smoke modeling frameworks, such as WRF-  
246 SFIRE (Mandel et al., 2011; Kochanski et al., 2016), WRF-Chem (Grell et al., 2005), and  
247 HRRR-Smoke directly account the transport of smoke within the dynamical core of the WRF.  
248 Other models, compute the transport of smoke in an offline setting, where output from a NWP  
249 model such as WRF, North American Mesoscale Forecast System (NAM) or the Global Forecast  
250 System (GFS) is used to trace the transport smoke. Smoke modeling frameworks such as  
251 HYSPLIT and CMAQ use the offline method. One benefit of the offline method is that the  
252 smoke modeler does not always need to run their own meteorological model, which can be  
253 timely and computationally expensive. However, this method does not allow two-way coupling

254 between the smoke and the atmosphere, which can sometimes be important when simulating the  
255 interactions between the smoke and meteorology (Kochanski et al., 2019). Smoke models, such  
256 as VSMOKE preclude the use of NWP models, and simply assume that the wind fields are  
257 steady state, therefore using wind data from a nearby weather station.

#### 258 *2.4 Aerosol physics*

259 Smoke particles directly interact with energy from the sun by scattering and absorbing  
260 incoming solar radiation due to the presence of black and organic carbon (Figure 1). Interactions  
261 between smoke particles and incoming solar radiation can result in differential heating of the  
262 atmosphere that can impact atmospheric stability and/or near-surface temperatures, i.e., aerosol  
263 direct effects (Bauer and Menon, 2012). For example, smoke shading effects occurs when  
264 incoming energy from the sun is blocked by the opaque smoke plume, which results in cooling at  
265 the surface (Robock, 1988; 1991; Trentmann et al., 2006). Smoke shading can impact  
266 temperature forecasts, or in more extreme circumstances, it can affect smoke transport (Segal  
267 and Arritt, 1992; Kochanski et al. 2019). An observational-based field campaign in Northern  
268 California found evidence of smoke-induced density currents where differential solar heating  
269 between areas with and without smoke resulting in a self-propagating, surface-based smoke  
270 plume that opposed the ambient wind (Lareau et al., 2015). A modeling-based study carried out  
271 by Kochanski et al., (2019) found that localized reductions in incoming solar radiation within  
272 smoke-filled mountain valleys reduced surface temperatures while increasing temperatures near  
273 the top of smoke layer. In this scenario, there was evidence that smoke was responsible for  
274 cooling the surface, suppressing convective boundary layer growth, which effectively limited  
275 ventilation between the smoke-filled layer and the atmosphere. In turn, this resulted in an  
276 accumulation of smoke and subsequently, more cooling via a nonlinear feedback mechanism.

277 Smoke particles can also interact with atmosphere via indirect effects where smoke particles  
278 alter cloud microphysics (Lindsey et al., 2008; Lee et al., 2018). To summarize, smoke particles  
279 can promote the formation of additional cloud water droplets at the expense of larger cloud water  
280 droplets since cloud droplets have to compete for a finite amount of water vapor (Andreae et al.,  
281 2004). A simulation of a PyroCb in the Texas Panhandle found that the smoke particles played  
282 an important role towards enhancing the strength of the convective updraft (Zhang et al., 2019).  
283 These results were consistent with Grell et al. (2011) who also concluded that simulated  
284 convection over Alaska was stronger in the presence of smoke, albeit the convection produced  
285 less precipitation.

286 Several existing smoke modeling frameworks such as WRF-Chem, WRF-SFIRE, and  
287 HRRR-Smoke are equipped to deal with some of the interactions noted above. Other processes  
288 not previously discussed, such as wet and dry deposition represent important loss processes for  
289 atmospheric particles like smoke (Zhang et al., 2011; Saylor et al., 2019) and are parametrized  
290 within most smoke transport models that simulate particulate matter. WRF-Chem contains a full  
291 suite of aerosol parameterizations that can account for effects ranging direct aerosol effects to  
292 indirect effects that can impact cloud microphysics and PyroCb development (Grell et al., 2011;  
293 Zhang et al., 2019). GEOS-Chem is another popular aerosol transport model for simulating  
294 smoke transport and for quantifying the impacts of smoke on radiative forcing at the global scale  
295 (Christian et al., 2019).

296 A variety of methods are used within smoke models to simulate aerosol physics. For  
297 example, some aerosol schemes use the bulk method where only the total mass of the aerosol  
298 compound is known, therefore this is no information about the particle number and aerosol size  
299 distribution (Chin et al., 2000). While this method is simple, it is numerically efficient and

300 computationally cheaper to run. Modal aerosol schemes are slightly more complex in that they  
301 include aerosol size distributions using three or more modes that includes the Aitken,  
302 accumulation, and coarse modes (Liu et al. 2016b). The most sophisticated method for  
303 simulating aerosol physics is through a bin method where aerosols are distributed into many  
304 discrete size bins, which are simulated separately (Zaveri et al., 2007). Bin methods are typically  
305 computationally expensive to run.

306

### 307 *2.5 Chemistry*

308 Smoke plumes are made of a mixture of many chemically active species and aerosols such as  
309 nitrogen oxides ( $\text{NO}_x = \text{NO} + \text{NO}_2$ ), nitrous acid (HONO), volatile organic compounds (VOCs),  
310 which can impact air quality through the formation of ozone ( $\text{O}_3$ ), and secondary organic  
311 aerosols (SOA) (Andrea and Merlet, 2001; Akagi et al., 2011; Jaffe and Wigder, 2011;  
312 Kochanski et al., 2016; Brey and Fischer, 2016; Peng et al., 2020).  $\text{O}_3$  is formed through the  
313 chemical reaction between molecular oxygen ( $\text{O}_2$ ) and atomic oxygen ( $\text{O}(^3\text{P})$ ). The supply of  
314 atomic oxygen is driven by chemical reactions involving  $\text{NO}_x$  and non-methane organic  
315 compounds that simultaneously exposed to sunlight photo-dissociate creating  $\text{O}(^3\text{P})$ . Since  $\text{O}_2$  is  
316 abundant in the atmosphere,  $\text{O}_3$  production is typically limited by the availability of  $\text{NO}_x$ . The  
317 most common sources of  $\text{NO}_x$  are anthropogenic emission sources and wildfires (Finlayson-Pitts  
318 and Pitts, 1986).

319 Smoke plume chemistry is sensitive to several factors including time of day, meteorology,  
320 altitude, chemical composition of the plume, combustion efficiency, transport time, and nearby  
321 emission sources (Giglio, 2007; Jaffe et al., 2004; Lim et al., 2019; Peng et al., 2020). Smoke  
322 shading effects within the plume can also reduce  $\text{O}_3$  production by limiting photochemical

323 reactions (Jaffe and Wigder, 2011) producing molecular oxygen. The sequestration of  $\text{NO}_x$  as the  
324 smoke plume ages can also limit  $\text{O}_3$  production downwind of the fire (Tanimoto et al., 2008).  
325 Due to the complex and non-linear interactions between  $\text{O}_3$  and other chemical processes,  
326 accurately simulating  $\text{O}_3$  chemistry within smoke can be difficult (Jaffe and Wigder, 2011;  
327 Kochanski et al., 2016).

328 There are several existing modeling frameworks that have been used to both better  
329 understand smoke plume chemistry and to make air quality forecasts for chemical species such  
330 as  $\text{O}_3$ . The Community Multiscale Air Quality (CMAQ) model is a state-of-the-art air quality  
331 model that can simulate many atmospheric chemical processes related to gas, aqueous, and  
332 aerosol phase chemistry (Sarwar et al., 2011; 2013). Therefore, models such as CMAQ can  
333 simulate complex chemistry associated with  $\text{O}_3$  and SOA. Operational air quality modeling  
334 frameworks such as AIRPACT (<http://lar.wsu.edu/airpact/>) are based on the CMAQ model (see  
335 **Chapter 9**). CMAQ generally estimates anthropogenic emissions using the Sparse Matrix  
336 Operator Kernel Emissions (SMOKE; <https://www.emascenter.org/smoke/>) combined with fire  
337 emissions defined by the Satellite Mapping Automated Reanalysis Tool for Fire Incident  
338 Reconciliation (SmartFire2)–BlueSky framework (Larkin et al., 2009). WRF-Chem and WRF-  
339 SFIRE-Chem have also been used to simulate chemical reactions within wildfire plumes (Pfister  
340 et al., 2011; Kochanski et al., 2016). For example, work by Kochanski et al. (2016) integrated  
341 WRF-SFIRE with WRF-Chem’s Model of Ozone and Related chemical Tracers (MOZART;  
342 Emmons et al., 2010) chemical mechanism to forecast  $\text{O}_3$  for the 2007 Witch-Guejito Santa Ana  
343 fires. Chemical models such as WRF-Chem and CMAQ also need chemical boundary conditions  
344 from either a larger-scale chemical transport model or a data assimilation product that utilize  
345 satellite observations. This is covered more in-depth in **Chapter 7**.

346

347 **3. Smoke transport models**348 *3.1 Box model*

349 Box models are one of the simplest approaches used to simulate smoke exposure (Letteau  
350 1970). As suggested by the name, a box model assumes that air for a specified domain can be  
351 represented by a box, which is often bounded by the surface and the top of the PBL. Smoke  
352 within the box model is often assumed to be instantaneously diluted throughout the entire  
353 column, thus eliminating the need to simulate smoke dispersion and the fire plume rise. Because  
354 of relative simplicity of the underlying assumptions within a box model, these models are easy to  
355 run, and require limited computational resources (Goodrick et al., 2012).

356 Box models have been previously used for smoke management applications in mountain  
357 valleys, where the lateral boundaries of the box are bounded by valley walls. Research presented  
358 Brown and Bradshaw (1994) indicated that while box models struggle with predicting near-  
359 surface smoke concentrations from local fires, these models can be useful for assessing smoke  
360 loading within remote mountain valleys for prolonged smoke episodes. Another study by Pharo  
361 et al. (1976) found that box model tended to overestimate smoke concentrations near fires. It was  
362 hypothesized that overestimated smoke concentrations stemmed from the instantaneous dilution  
363 assumption made by box models, which is not valid in the vicinity of the fire where the plume  
364 dynamics and interactions with winds and atmospheric stability control mixing and dilution.

365 Zero-dimensional box models are also popular choice for simulating complex atmosphere  
366 chemistry within smoke plumes for research-based applications (Wolfe et al., 2016; Decker et  
367 al., 2021). Zero-dimensional box models are deployed by atmospheric chemists to investigate  
368 different chemical mechanisms (Archibald et al., 2010), analyze field observations (Decker et al.,

369 2021), and for laboratory chamber experiments (Paulot et al., 2009). The models are particularly  
370 useful for understanding specific chemical processes, developing conceptual models, and testing  
371 hypotheses through sensitivity experiments (Wolfe et al., 2016).

372

### 373 *3.2 Gaussian plume model*

374 The Gaussian plume model represents the simplest way for simulating the downwind  
375 transport of smoke. Instead of letting smoke dilute within a targeted domain like what is done for  
376 box models, the Gaussian plume model attempts to account for atmospheric transport and  
377 dispersion (Taylor, 1922). Crosswind transport, i.e., dispersion is parameterized as a Gaussian  
378 distribution that takes the form of a steady state solution of the advection-diffusion equation. The  
379 direction of the smoke transport is determined by the wind speed and direction. Since winds are  
380 assumed to be constant in time and space, smoke is assumed to travel in a straight line from  
381 where it is emitted until it reaches the end point of the smoke plume or model domain. As a  
382 result, areas that frequently experience highly variable weather phenomena such as sea breezes,  
383 frontal passages, and mountain-valley circulations may not be appropriate for a Gaussian plume  
384 model. However, for cases where meteorological conditions are homogenous, Gaussian plume  
385 model models can be an ideal tool for simulating downwind horizontal smoke transport given the  
386 limited computational demands and model inputs for these models.

387 As of today, there are two smoke models that utilize Gaussian plume theory to simulate  
388 smoke transport and exposure. VSMOKE (Lavdas, 1996) is often used by land managers in the  
389 Southeastern U.S. to provide a quick and simple estimate of smoke impacts for prescribed burns  
390 based on planned fire activity and weather forecasts (Jackson et al., 2007). No wildfire plume  
391 rise is used within VSMOKE, thus the user must specify a fraction of smoke that is released near

392 the ground and at the PBL. For smaller prescribe burns, its generally safe to partition most of the  
393 smoke emissions within the PBL. However, for larger prescribe burns and wildfires, this  
394 assumption could be inadequate, as the fire plume rise can sometimes inject smoke into the free  
395 troposphere (Banta et al., 1992). The Simple Approach Smoke Estimation model (SASEM;  
396 Sestak and Fiebau, 1988) is another Gaussian plume model that was designed to estimate smoke  
397 transport across relatively flat terrain. Like VSMOKE, SASEM can estimate ground-level smoke  
398 concentrations. SASEM can also estimate visibility impairment and the height of the fire plume  
399 rise as predicted by the Briggs (1975) plume rise model (see **Section 4b**). SASEM is mostly used  
400 for prescribed burns in the state of Arizona (Goodrick et al., 2012).

401

### 402 *3.3 Puff models*

403 Puff models represents another class of dispersion models, which reduces the number of  
404 assumptions made by Gaussian plume models (Lin, 2012). The Puff model represents the smoke  
405 plume as a collection of independent smoke “puffs” that are assigned an average smoke  
406 concentration that is representative of the puff’s volume. Puffs are constantly released  
407 throughout the duration of a burn, with each puff having a total mass of smoke that is related to  
408 the smoke emissions at the time of when the puff was emitted from the fire (Goodrick et al.,  
409 2012). Once the puffs are released into the atmosphere, they are transported by winds that can  
410 vary in time and space, unlike Gaussian plume models. Since Puff models follows a fluid parcel  
411 as it travels through time and space, e.g., moving reference frame, these models are classified as  
412 being Lagrangian.

413 Puff models are well suited for areas with lots of variability in winds such as mountainous  
414 areas and coastlines. The effects of diffusion and entrainment are also accounted by Puff models.

415 For cases where the Puff's volume increases, the smoke concentration within the Puff would  
416 decrease, while a decrease in the Puff's volume would correspond in an increase in smoke  
417 concentration. While Puff models represent a significant step forward relative to Gaussian plume  
418 modeling approaches, areas with strong wind shear and turbulence can distort puffs into non-  
419 Gaussian shapes (Lin, 2012). In these situations, ad hoc parameterizations such as puff splitting  
420 or merging are often necessary (Walcek, 2002).

421 CALPUFF (Scire et al. 2000) and Hybrid Single-Particle Lagrangian Integrated Trajectory  
422 (HYSPLIT; Draxler and Hess, 1997) are the most commonly used model frameworks that utilize  
423 Puff models. The CALPUFF model is driven by a diagnostic meteorological model (CALMET)  
424 that grids variables such as winds, temperature, PBL heights, friction velocity, and the Monin  
425 Obukhov length on a three-dimensional micrometeorological domain. The three-dimensional  
426 data is either obtained by interpolating meteorological data from nearby near-surface and upper-  
427 air observations and/or from a Eulerian NWP model. CALPUFF is commonly used by the  
428 Environmental Protection Agency to assess the impact of atmospheric pollutants on air quality  
429 for an area of interest (Scire et al., 2000). Even though CALPUFF does not explicitly resolve the  
430 plume rise, it utilizes the Brigg plume rise parameterization to estimate the injection height of  
431 atmospheric pollutants. Several studies have used CALPUFF for assessing the impacts of fires  
432 on different airsheds across North America. In one study, CALPUFF was used to quantify the  
433 impacts of agriculture burning for areas along the USA-Mexico border (Choi and Fernando,  
434 2007). Converting fire activity, fuel conditions, and burn time into smoke emissions was listed as  
435 one of the major limitations of simulating smoke with CALPUFF. Jain et al. (2007) found that  
436 smoke plumes from agriculture burns in the Pacific Northwest exhibit large variability and were  
437 sensitive to fire input parameters when using CALPUFF. Despite the uncertainties associated

438 with meteorology and fire input parameters, CALFPUFF was mostly able to reproduce surface  
439  $PM_{2.5}$  concentrations when evaluated with nearby air quality stations.

440 HYSPLIT is another modeling framework that can be used to simulate the transport of  
441 pollutants as puffs, single trajectories, or an ensemble air parcel trajectories, with the latter being  
442 discussed more in **Section 3d**. Similar to CALPUFF, an external three-dimensional NWP model  
443 needs to provide meteorological inputs such as temperature and wind to determine transport  
444 pathways for puffs within HYSPLIT. A joint project between the United States National Oceanic  
445 and Atmospheric Administration (NOAA) and the Australia's Bureau of Meteorology led to the  
446 implementation of several modules, which allow HYSPLIT to account for chemical reactions in  
447 the atmosphere. HYSPLIT's puff model assumes that puffs continuously grow until they reach a  
448 size threshold that is larger than the meteorological grid cell. Once puffs reach the size threshold,  
449 they are split up into smaller puffs with identical properties in terms of pollutant concentrations.

450

#### 451 *3.4 Lagrangian Particle Dispersion models*

452 While Puff models can account for changing flow fields, these models make many  
453 assumptions regarding the expansion and contraction of the puff, along with interactions between  
454 different puffs. Lagrangian particle dispersion models (LPDMs) attempt to rectify some of these  
455 issues by simulating atmospheric transport as an ensemble of particles, with each particle  
456 representing a parcel of air with equal mass. These particles possess several important properties  
457 such as (1) being small enough where they can follow the wind field without becoming  
458 deformed, but (2) much larger than the average distance between air molecules, and (3) have  
459 fluid properties that are nearly identical to the surrounding air; thus, are unaffected by  
460 gravitational settling and/or buoyancy (Lin, 2012). These particles are transported by the mean

461 wind ( $\bar{\mathbf{u}}$ ) and a stochastic turbulent component ( $\mathbf{u}'$ ), which can be parameterized as a Markov  
462 process (Lin, 2012). As a result, these models are well-equipped to handle cases with strong  
463 turbulence and/or wind shear. Simulated particles can also be referred to as trajectories. Since  
464 LPDM models must use thousands of particles to accurately depict turbulent dispersion (Mallia  
465 et al., 2015), these models are more computationally expensive than puff models. However, the  
466 downside of the added computational cost of simulating thousands of particles through three-  
467 dimensional space is generally outweighed by LPDM's ability to naturally simulate the effects of  
468 turbulence and wind shear. Several LPDM models are currently used to simulate smoke from  
469 prescribed burns to reduce human exposure to smoke or used for research-based applications.  
470 For example, LPDMs have been deployed in inverse-based studies to better understand  
471 spatiotemporal variability of fire emissions (Kim et al., 2020). LPDM models have also been  
472 used to identify major source regions of wildfire smoke and to quantify the role of the wildfire  
473 plume rise on smoke transport (Mallia et al., 2015; 2018).

474 FLEXPART (Stohl and Thomson, 1999) is a LPDM model that simulates long-range  
475 atmospheric transport and dispersion for a many atmospheric pollutants, tracers, and greenhouse  
476 gases. FLEXPART parameterizes the effects of wet and dry deposition. FLEXPART was first  
477 applied to wildfire smoke by Wotawa and Trainer (2000), who used FLEXPART to examine the  
478 impacts of Canadian wildfires on air quality in the southeastern U.S. Based on simulated results  
479 from FLEXPART, Wotawa and Trainer (2000) found that wildfire smoke was large responsible  
480 for elevated concentrations of carbon monoxide (CO) during the summer of 1995. FLEXPART  
481 was integrated with the National Observatory of Athens FireHub platform  
482 (<http://ocean.space.noa.gr/fires>) to simulate smoke plumes over Greece. An analysis carried out  
483 Solomos et al. (2015) found that FLEXPART, driven by winds from WRF, was able to capture

484 long-range smoke transport over Greece, along with transport near complex terrain features such  
485 as mountains and coastlines. A column-based plume rise model was integrated within  
486 FLEXPART to handle the vertical transport of smoke due to the fire plume rise.

487 DaySmoke (Achteimeir et al., 2011) is another model that uses Lagrangian-based framework  
488 to simulate downwind smoke transport. DaySmoke was originally built off the ASHFALL  
489 model, which was used to simulate deposition of ash particles from agriculture fires. Today,  
490 DaySmoke is used to simulate smoke dispersion to limit smoke exposure of communities  
491 downwind of prescribed burns. DaySmoke consists of 4 components for simulating smoke,  
492 including an entraining torrent model, a detraining particle model, a large eddy parameterization  
493 used to simulate the PBL, and a smoke emissions model, which describes the emission history  
494 prescribed burns. The entraining torrent model handles the effects of convective uplift from the  
495 fire plume rise. In addition, the convective updraft within DaySmoke can be separated into multi-  
496 core updrafts, which have weaker updrafts, smaller diameters, and are more sensitive to the  
497 entrainment. Ultimately, the separation of the convective updraft into multiple cores can limit the  
498 altitude at which smoke is injected, thus correctly specifying the number of updraft cores is  
499 critical when simulating the fire plume rise (Liu et al., 2010). Once the smoke particles are  
500 discharged from the smoke plume, they are traced through the atmosphere by a mean and  
501 turbulent wind component (Achteimeir et al., 2011). Like other LPDM models, the turbulent or  
502 convective mixing component is considered stochastic. Since DaySmoke employs relatively  
503 simple physics and no chemistry, the model requires less computational resources relative to  
504 other smoke modeling frameworks.

505 HYSPLIT is a popular tool for simulating smoke transport at larger scales (10-1000 km), and  
506 can be run as a LPDM or, as previously mentioned as a puff model, depending on the options

507 selected at runtime (Draxler and Hess, 1997). HYSPLIT has been integrated with the BlueSky  
508 modeling framework (Larkin et al., 2009; O'Neill et al., 2008), which utilizes fuel maps and fire  
509 consumption rates to estimate smoke emissions ([https://www.arl.noaa.gov/hysplit/smoke-](https://www.arl.noaa.gov/hysplit/smoke-prescribed-burns/)  
510 [prescribed-burns/](https://www.arl.noaa.gov/hysplit/smoke-prescribed-burns/)). The meteorology used to drive HYSPLIT trajectories generally comes from  
511 an external NWP model such as the many model outputs provided by the National Centers for  
512 Environmental Prediction (NCEP).

513 The Stochastic Time-Inverted Lagrangian Transport (STILT) model (Lin et al. 2003), which  
514 is based off HYSPLIT and has since been merged back with HYSPLIT (Loughner et al., 2021) is  
515 another LPDM that has been used to simulate the impacts of smoke on air quality across the  
516 Western U.S. (Mallia et al., 2015). Smoke emissions used by STILT can be vertically distributed  
517 using the Freitas plume rise model (Freitas et al., 2007; Mallia et al., 2018). STILT typically uses  
518 'backward' trajectories to determine the origin of air that is arriving at a receptor location.  
519 Backward trajectories can be used to derive the footprint for a receptor which can then be  
520 mapped with smoke emissions to determine contributions of smoke from upwind fires (Figure  
521 2a). The receptor-orientated approach used by STILT makes this modeling framework  
522 particularly useful for identifying fires responsible for deteriorating air quality as seen in Figure  
523 2b. Since the NWP models used to drive backward trajectories are often imperfect, STILT has  
524 the unique ability to translate wind errors into modeled smoke uncertainties (Figure 2b) (Mallia  
525 et al., 2015).

### 526 *3.5 Eulerian grid models*

527 Smoke transport can also be simulated from the Eulerian perspective where instead of  
528 following a puff or particle in a moving coordinate system, a Eulerian 'grid model' simulates  
529 smoke transport on a fixed reference plane. A Eulerian model can be visualized as collection of

530 individual cubes that are stacked within a large box, with the box being representative of the  
531 lateral boundaries of the model. Equations used to describe the transport of smoke are then  
532 solved for each individual cube, which is often referred to as a model grid cell. While tracking  
533 individual smoke plumes with a Eulerian based model can be more difficult, grid models are  
534 more suited for simulating interactions between different plumes and for determining how  
535 anthropogenic emission sources might interact with these plumes to form secondary pollutants  
536 like O<sub>3</sub> (Goodrick et al., 2012). Eulerian grid models heavily rely on NWP models to determine  
537 how smoke is transported throughout the model domain. Meteorological data can be provided as  
538 an input for Eulerian-based smoke models or smoke transport and chemistry can be solved inline  
539 with the meteorology. One potential limitation of Eulerian-based frameworks is that emissions  
540 are assumed to be instantaneously diluted through model grid cells, which can be unrealistic,  
541 especially in coarser-scale model simulations (Goodrick et al., 2012).

542 CMAQ is a state-of-the-art air quality model, which is one of the most widely used tools for  
543 air quality applications. Such applications include regulatory and policy analysis, research, and  
544 operational forecasting (Byun and Schere, 2006; Baker et al., 2018). CMAQ contains a suite of  
545 atmospheric chemistry and emission routines that enables the model to simulate smoke-related  
546 chemical and aerosol processes such as photochemistry, SOA formation, and advanced aerosol  
547 physics. While CMAQ does not simulate its own meteorology, NWP model data can be provided  
548 as an input, or the model can be coupled directly with the WRF model (Zou et al., 2019).  
549 Routines exist within CMAQ, where smoke can be injected between two specified vertical levels  
550 either by the user or by an offline plume rise model. AIRPACT (<http://lar.wsu.edu/airpact/>),  
551 which is an operational model used to make air quality forecasts across the Pacific Northwest, is  
552 an example of an air quality modeling system that uses CMAQ driven by an external WRF

553 model and fire emissions generated from BlueSky. More details on AIRPACT can be found in  
554 the **Chapter 9**.

555 Another popular choice for simulating smoke is with WRF-Chem, which is a chemical  
556 transport modeling framework that can simultaneously model meteorology, aerosol physics, and  
557 chemical transformations in the atmosphere (Grell et al., 2005). Since the chemical and aerosol  
558 modules within WRF-Chem are directly coupled with the dynamical core and physical  
559 parameterizations, smoke emissions can modify weather conditions through smoke shading  
560 and/or cloud microphysical processes. This type of coupling is unique to modeling frameworks  
561 like WRF-Chem, where smoke simulations are computed in-line with meteorology.

562 Smoke emissions within WRF-Chem are typically provided by an external emission  
563 inventory such as Fire Inventory from NCAR (FINN; Weidenmeyer et al., 2010), while smoke  
564 can be vertically distributed within WRF-Chem using the Freitas et al. (2007) plume rise model.  
565 A study by Grell et al. (2011) found that smoke emissions had the potential to affect mesoscale  
566 (10-100 km) weather patterns across Alaska by changing vertical temperature and moisture  
567 profiles in areas absent of cloud cover. Sensitivity tests also revealed that high concentrations of  
568 PM<sub>2.5</sub> were responsible for altering cloud microphysical processes, which ultimately impacted  
569 the modeled spatiotemporal distribution of precipitation across Alaska in 2004. The National  
570 Oceanic and Atmospheric Administration (NOAA)'s operational smoke forecast system, HRRR-  
571 smoke is based on WRF-Chem v3.9, with several in-house modifications related to smoke  
572 aerosol physics (Amohdavi et al., 2017). More details on HRRR-smoke can be found in **Chapter**  
573 **9**.

574 Global-scale simulations of smoke transport can be achieved with modeling frameworks such  
575 as GEOS-Chem (<http://acmg.seas.harvard.edu/geos/>), which has been used in previous work to

576 isolate the impacts of wildfire smoke on global climate and air quality (Christian et al., 2019; Li  
577 et al., 2020). Like CMAQ and WRF-Chem, GEOS-Chem includes chemical and aerosol routines  
578 to simulate changes in the chemical composition of the atmosphere (Bey et al., 2001).  
579 Meteorology for GEOS-Chem is provided as an input from an external global NWP model,  
580 while smoke emissions are estimated using GFED or FINN. Since GEOS-Chem is a global  
581 model, the horizontal grid spacing within the model is very coarse relative to the grid spacing of  
582 the other models presented in this chapter. Despite having a coarser model resolution, GEOS-  
583 Chem is one of the few models specifically designed to simulate the large-scale impacts of  
584 smoke on global air quality, weather, and climate.

585

### 586 *3.6 Coupled fire-atmosphere models*

587 Advancements in computational facilities have led to the development and deployment of  
588 coupled fire-atmosphere models. Like Eulerian grid models, these coupled fire-atmosphere  
589 models simulate smoke transport on a three-dimensional grid. Coupled-fire atmosphere models  
590 also simulate their own meteorology using a computational fluid dynamics weather prediction  
591 model. Unlike some of the Eulerian grid models discussed in the previous section, coupled fire-  
592 atmosphere models simulate fire progression using a formula that parameterize fire growth based  
593 on local meteorology, terrain, and fuel characteristics (Mandel et al., 2011), or through the  
594 explicit representation of combustion processes (Mell et al., 2007; Mell et al., 2010; Linn et al.,  
595 2002; Linn and Cunningham, 2005).

596 Coupled fire-atmosphere models can utilize information about the predicted burned area and  
597 fuel loading to forecast fuel consumption, heat fluxes, and smoke emissions. The heat fluxes  
598 forecasted by these models can also dynamically interact with the atmosphere, which allows

599 coupled-fire atmosphere models to explicitly simulate phenomena such as the wildfire plume rise  
600 (see **Section 4d**) and fire-induced winds near the fire front. Some coupled fire-atmosphere  
601 models such as WRF-SFIRE can simulate the impacts of smoke on meteorology through aerosol  
602 physics and chemistry coupling (Kochanski et al. 2016; Kochanski et al. 2019). While coupled  
603 fire-atmosphere models represent the most sophisticated way to simulate smoke, these models  
604 can be computationally demanding compared to other models due to the computations needed to  
605 resolve near-fire circulations and plume dynamics. However, multi-scale coupled fire-  
606 atmosphere models such as WRF-FIRE and WRF-SFIRE use a nested domain setup that allows  
607 these models to embed small-scale, high-resolution domains within larger and coarser  
608 computational domains. Ultimately, this allows modeling frameworks like WRF-FIRE and  
609 WRF-SFIRE to simulate smoke dispersion across large distances at a relatively lower  
610 computational cost. Outside of forecasting applications, coupled fire-atmosphere models are  
611 ideal tools for studying how fire and fire behavior dynamically interacts with the atmosphere.

612 FIRETEC and WFDS use a finite-volume, large eddy simulation to model fine-scale  
613 meteorological flows near the fire of interest. Here, large eddies within turbulent flow are  
614 explicitly resolved by within the numerical grids of FIRETEC and WFDS, while smaller eddies  
615 are parameterized with sub-grid scale models (Mell et al., 2007; Linn and Cunningham, 2005).  
616 Typically, the grids used by FIRETEC and WFDS are on the order of meters. Since FIRETEC  
617 and WFDS use a physics-based approach for simulating fire growth and combustion, detailed  
618 information about fuels and fuel density on a scale  $\sim 1$ -m is needed. This attention to detail comes  
619 at a cost as FIRETEC and WFDS simulations are computationally expensive to run. Therefore,  
620 these models are only feasible for research-based applications. Furthermore, the model grid  
621 spacing used within FIRETEC and WFDS also limits these models to individual fire-scale

622 problems that are typically less than 100 acres in size. Due to the domain size limitations  
623 associated with FIRETEC and WFDS, these models are better suited for describing fire behavior  
624 and hyper-local smoke transport (Liu et al. 2019). While models such as FIRETEC and WFDS  
625 can represent detailed combustion processes and the fire-atmosphere interactions, they do not  
626 account for the microphysical and radiative impacts of smoke on the atmosphere or chemical  
627 transformations of smoke downwind from the fire.

628 Models such as WRF-FIRE and WRF-SFIRE operate on a slightly different scale than  
629 FIRETEC and WFDS, so that they can be used in both research and forecast applications. To  
630 reduce computational costs, fire growth within WRF-FIRE and WRF-SFIRE is parameterized  
631 using an empirical formula instead of taking a physics-based approach (Mandel et al., 2011; Liu  
632 et al., 2019). While models such as WRF-FIRE and WRF-SFIRE parameterize fire growth rates,  
633 heat fluxes generated from the modeled fire are dynamically coupled to the atmosphere.  
634 Typically, these models resolve fire progression on scales on the order of tens of meters, while  
635 the meteorology from WRF, which is used to drive the fire and simulate smoke transport, is  
636 solved on grid with a horizontal grid spacing between 400-1,300m (Kochanski et al., 2019). This  
637 allows models such as WRF-FIRE and WRF-SFIRE to simulate smoke across a larger domain  
638 compared to FIRETEC and WFDS. In addition, WRF-based modeling frameworks use a nested  
639 domain configuration where meteorology and smoke simulated in the innermost domain centered  
640 on the fire is fed into subsequently coarser, but larger domains. Despite using a coarser  
641 atmospheric grid relative to FIRETEC and WFDS, both WRF-FIRE and WRF-SFIRE can  
642 explicitly resolve the wildfire plume rise and first order fire-atmosphere interactions (Liu et al.,  
643 2019). Both models treat smoke as a passive tracer, with smoke emissions being estimated based  
644 on the fuel consumed by the simulated fire.

645 WRF-SFIRE was recently coupled to WRF-Chem to allow smoke generated by the fire to  
646 undergo chemical transformations while smoke aerosols can be scavenged from the atmosphere.  
647 Coupling with the WRF-Chem's aerosol model (GOCART) also allows smoke to interact with  
648 atmospheric radiation, therefore allowing WRF-SFIRE to account for smoke shading effects.  
649 This type of coupling is unique to only WRF-SFIRE. Preliminary work carried out by Kochanski  
650 et al. (2016) found that WRF-SFIRE, coupled with WRF-CHEM was able to reproduce elevated  
651 concentrations of  $\text{NO}_x$  and  $\text{PM}_{2.5}$  for two large fires in Southern California during the 2007 fire  
652 season. A follow up study by Kochanski et al. (2019) found that WRF-SFIRE simulations were  
653 able to capture smoke shading effects within mountain valleys across northern California. A  
654 positive feedback mechanism was also identified where smoke aerosols resulted in cooler  
655 temperature at the surface, which allowed additional smoke aerosols to accumulate at the base of  
656 mountain valleys. WRF-SFIRE simulations coupled with WRF-Chem were also used to forecast  
657 a wildfire smoke event in Salt Lake City, UT during the summer of 2018. WRF-SFIRE smoke  
658 simulations during this event were able to skillfully capture the orientation and shape of the  
659 plume, along with local-scale nocturnal mountain valley circulations (Figure 3) (Mallia et al.,  
660 2019).

661

## 662 **4. Plume-rise models**

### 663 *4.1 Simplified approaches*

664 Earlier smoke modeling frameworks often assumed that smoke from biomass burning was  
665 either injected at a fixed altitude, evenly distributed throughout the PBL (Pfister et al., 2008;  
666 Hyer and Chew, 2010), assumes some type of ratio for partitioning emissions between the PBL  
667 and free troposphere (FT) (Turquety et al., 2007; Leung et al., 2007; Elguindi et al., 2010), or is

668 prescribed based on local measurements such as satellite (Chen et al., 2009). For continental-  
669 scale smoke simulations across North America, the vertical distribution of smoke was found to  
670 be insensitive to the modeled plume injection height. It was hypothesized by Chen et al. (2009)  
671 that strong summertime convection tends to mix smoke throughout the troposphere, which  
672 limited the influence of the plume injection height on vertical smoke distributions.

#### 673 *4.2 Empirical*

674 Another way to estimate the plume injection height is through empirically based models,  
675 which require inputs such as buoyancy, fire power, fire area, and/or generalized characteristics of  
676 the atmosphere such as atmospheric stability or the PBL height.

677 The Briggs equations (Briggs, 1975), which is one of the first plume injection models, was  
678 originally developed to estimate the height of plumes released from smokestacks. Today, the  
679 Briggs equations are commonly used by smoke modeling frameworks such as CMAQ, BlueSky  
680 and HYSPLIT. The Briggs model consists of a series of equations used for different stability  
681 conditions and whether the plume is momentum or buoyancy dominated. The plume injection  
682 height estimated by the Briggs model is a function of buoyancy, ambient wind speeds, and  
683 stability. Since the Briggs formulas contain no direct input for the fire heat release, the fire heat  
684 release needs to be converted into a buoyancy flux (Raffuse et al., 2012). Plume rise results with  
685 the Briggs model have been mixed, which is reasonable considering that it was originally  
686 developed to model plumes from smokestacks. Work by Raffuse et al. (2012) and Gordon et al.  
687 (2018) found that the Briggs model typically underestimated plume rises, especially for larger  
688 wildfires. Achtemeier et al. (2011) hypothesized that models like Briggs are unable to account  
689 for microphysical impacts such as latent heat releases. As a result, the Briggs model is unable to  
690 account for extreme pyroconvection like pyrocumulus or pyrocumulimbus clouds. However,

691 Achtemeier et al. (2011) suggests that the Briggs model may perform better for smaller wildfires  
 692 and prescribed burns.

693 A newer methodology for estimating wildfire smoke plume heights was presented in (Sofiev  
 694 et al., 2012). Like the Briggs models (Briggs, 1975), this methodology uses a semi-empirical  
 695 formula to estimate fire plume tops. This parameterization uses an energy-balance-based  
 696 approach to estimate plume tops, similar to convective cloud parameterizations used within  
 697 larger-scale atmospheric models. The plume height within the Sofiev et al. (2012) scheme is  
 698 estimated from the following:

$$699 \quad H_p = \alpha z_i + \beta \left( \frac{FRP}{P_{f0}} \right)^\gamma \exp\left( \frac{-\delta N_{FT}^2}{N_0^2} \right)$$

700 where  $\alpha$  is part of the PBL passed freely,  $\beta$  weights the contribution of fire intensity,  $\gamma$   
 701 determines the power-law dependence on the fire radiative power ( $FRP$ ),  $\delta$  weights the  
 702 dependence of the stability of the FT on the plume rise height ( $H_p$ ),  $P_{f0}$  is the reference fire  
 703 power ( $P_{f0} = 10^6$  W),  $N_0^2$  is the Brunt-Vaisala frequency reference number ( $N_0^2 = 2.5 \times 10^{-4}$  s<sup>-2</sup>),  
 704 and  $N_{FT}^2$  is the Brunt-Vaisala frequency of the FT. A learning subset of satellite fire smoke plume  
 705 observations from the Multi-angle Imaging SpectroRadiometer (MISR) were then used to  
 706 determine the value of the empirical calibration constants ( $\alpha$ ,  $\beta$ ,  $\gamma$ ,  $\delta$ ) where  $\alpha$  represents is the  
 707 part of the plume that passes freely through the PBL,  $\beta$  accounts for the weighted contribution  
 708 from the fire intensity,  $\gamma$  quantifies the power-law dependence of the fire's FRP on the plume  
 709 height, and  $\delta$  defines the plume top dependence on the atmospheric stability within the free  
 710 troposphere.

711 Results in Sofiev et al. (2012) found that their methodology outperformed both the Briggs  
 712 and 1-D column models when applied to 2000 fire plumes from an independent MISR database

713 across North America and Siberia. One potential limitation of this model is that the parameters  
714 defined in Sofiev et al. (2012) are primarily tuned for shallower smoke plumes, since the training  
715 data set to develop the parameters only included plume rises with heights less than 4-km  
716 (Paugnam et al., 2016).

717

#### 718 *4.3 Column models*

719 Another way for estimating plume top heights is through one-dimensional column models  
720 such as the Freitas et al. (2007; 2010) model. The Freitas plume rise model is based off a plume  
721 model developed by Latham (1994), which simulates the wildfire plume rise using the equations  
722 for vertical momentum, first law of thermodynamics, mass continuity, and cloud microphysics.  
723 In addition, the effects of entrainment near the edges of the plume are also parameterized as two  
724 entrainment coefficients, with one accounting for the effects of turbulence plume edge, and the  
725 other describing for ambient wind shear effects. The final plume injection height is often used  
726 within chemical and smoke transport models such as WRF-CHEM (Grell et al., 2005; Pfister et  
727 al., 2011; Sessions et al., 2011), STILT (Mallia et al., 2018), and HRRR-smoke. One added  
728 benefit of a column-based approach is that this method can provide the vertical plume  
729 characteristics, in addition to the final injection height (Figure 4). The final injection height is  
730 typically assumed when the upward vertical velocity  $w$  reaches  $0 \text{ m s}^{-1}$ . Since the Freitas plume  
731 rise model is cloud resolving, it can simulate moist pyroconvection. The Freitas model's ability  
732 to simulate moist pyroconvection can be seen in Figure 4, which shows a secondary increase in  
733 vertical velocity between 2.5 – 5 km that is collocated with an increase in liquid cloud water and  
734 latent heat releases.

735 Inputs for the Freitas plume rise model includes a one dimensional profile of ambient

736 atmospheric conditions such as temperature, relative humidity, and wind speed, along with  
737 surface boundary conditions provided by the fire, i.e., heat flux and fire area. Natively, the  
738 Freitas model assumes fire heat fluxes and area based on the vegetation type that is being burned.  
739 The heat flux and fire area are then used to compute a buoyancy flux ( $F$ ) following the  
740 expression derived by Viegas et al. (1998):

$$741 \quad F = \frac{gR}{c_p p_e} r^2$$

742 where  $g$  is equal to the gravity constant ( $g = 9.81 \text{ m s}^{-1}$ ),  $R$  represents the ideal gas constant ( $R =$   
743  $287 \text{ J K}^{-1} \text{ kg}^{-1}$ ,  $c_p$  denotes specific heat at a constant pressure ( $c_p = 1004 \text{ J kg}^{-1}$ ),  $p_e$  is the ambient  
744 surface pressure, and  $r$  defines the radius of the fire. The buoyancy flux can be used to compute  
745 the near-surface vertical wind velocity and temperature.

746 More recent work by Val Martin et al. (2012) tried alternative methods for prescribing fire  
747 input parameters, such as using satellite FRP to estimate sensible heat fluxes and aggregating  
748 satellite fire pixels to construct burned areas. This method resulted in slightly improved  
749 simulated plume rises when compared to satellite observations, however, the authors note the  
750 Freitas model was unreliable for identifying plumes that were injected into the FT. It was  
751 hypothesized that model errors in plume rises likely stemmed from uncertainties surrounding fire  
752 input parameters rather than plume rise model formulation. A study conducted by Mallia et al.  
753 (2018) showed the Freitas model was able to realistically capture the plume rise for an  
754 extensively instrumented prescribed burn in Eglin Airforce Base, FL, when driven by observed  
755 fire heat fluxes and burned area. It should be noted however, that this analysis was carried out for  
756 a single case study, for a relatively small burn (area =  $1.51 \text{ km}^2$ ), where no pyroCu or Cb activity  
757 was observed.

758

759            *4.4 Fully physical three-dimensional representation of plume dynamics*

760            Continued advancements in computational resources have resulted in a newer generation  
761 smoke models that can explicitly resolve wildfire plume rises. For the full physics method, heat  
762 fluxes from the fire are injected directly into the near-surface grid cells of a high-resolution  
763 three-dimensional atmospheric model (Goodrick et al., 2012). Like the column-based approach,  
764 the atmosphere will respond to the fire heating by generating a buoyant convective plume. One  
765 way that this approach different from the column-based approach is that here the plume is  
766 resolved in three-dimensional space instead of one-dimensional. In addition, these models  
767 typically run at a fine enough resolution where key processes such as entrainment, multiple  
768 plume cores, pyroconvection and upward smoke transport are directly simulated by the model,  
769 instead of being parameterized. The full physics approach typically requires the model to have a  
770 sufficiently fine grid-spacing so that the model can explicitly resolve plume rise dynamics while  
771 simultaneously having the volume needed to encompass the convective plume (Goodrick et al.,  
772 2012). As such, short model time steps, combined with fine grid cells, often covering a large  
773 volume, can drastically increase computational resources needed to explicitly resolve the wildfire  
774 plume rise.

775            Directly simulating the wildfire plume rise using a fully physical approach was first  
776 pioneered by Trentmann et al. (2006) and Luderer et al. (2006), who used a high-resolution  
777 atmospheric model to simulate extreme pyroconvection over the Chisholm wildfire located in  
778 Alberta, Canada. The plume rise associated with the Chisholm wildfire reached an altitude of 13-  
779 km, according to radar observations. The plume rise simulations carried out by Trentmann et al.  
780 (2006) and Luderer et al. (2006) were able to replicate the intense pyroconvection observed  
781 during this event while also illustrating how meteorological dynamics are coupled with large

782 wildfires. Coupled fire-atmosphere models such as WRF-SFIRE and WRF-FIRE also explicitly  
783 resolve the wildfire plume rise. WRF-SFIRE simulations conducted by Kochanski et al. (2016;  
784 2018) and Mallia et al. (2020a) found that modeled plume top heights compared reasonably well  
785 to satellite-estimated plume heights (average error =  $\pm 500$  m). An example of a full physics  
786 simulation of a wildfire plume rise by WRF-SFIRE can be seen in Figure 5.

787

## 788 5. Summary

789 The number of large and devastating fires are expected to increase in the coming decades,  
790 which will expose communities to poor air quality. Therefore, smoke models will be an  
791 important tool for limiting the public's exposure to degraded air quality through smoke forecasts  
792 and for determining the optimal time for igniting prescribed burns. Wildfires are also projected  
793 to emit more aerosols into the atmosphere, which can affect weather and climate if the smoke is  
794 injected high up into the atmosphere (Peterson et al., 2018).

795 Within this chapter, we've provided a brief introduction to the different types of smoke  
796 models that are available for researchers, and air quality and land/fire managers alike. This  
797 chapter reviews models that range from simple box and Gaussian plume models to more  
798 sophisticated modeling systems that can simulate smoke on an atmospheric grid with full physics  
799 and photochemistry. Also provided in this chapter is an in-depth discussion on coupled fire-  
800 atmosphere models, which has not been included in other review articles. This chapter also  
801 reviews processes that are important in the context of smoke transport and how these  
802 fundamental processes are resolved within smoke modeling frameworks.

803 While we attempt to cover all smoke models that are available to researchers and managers,  
804 covering every smoke model in existence would prove to be an exhaustive effort that could

805 probably be a book in itself! Nonetheless, we attempt to present a description of a diverse range  
806 of smoke transport and dispersion models to the reader. Ultimately, there is no smoke modeling  
807 tool that can be treated as a “silver bullet” as each of the models presented here have strengths  
808 and weaknesses that are dependent on the application that the model is being used for. Thus, we  
809 emphasize that determining the best smoke model for any given application will be dependent on  
810 the needs of the user and *what they need* the smoke model to do.

811

## 812 **6. Future directions**

813 Fundamentally, the processes that govern smoke transport and dispersion are well  
814 understood, especially in the absence of significant pyroconvection (Goodrick et al., 2012).  
815 However, processes related to the fire plume rise (Val Martin et al., 2012; Paugnam et al., 2016),  
816 aerosol microphysics (Forrister et al., 2015; Xie et al., 2018), and plume chemistry (Jaffe and  
817 Widger, 2011) are less understood. Recent field campaigns such as the NASA-NOAA FIREX-  
818 AQ campaign and Joint Fire Science’s Fire Smoke and Model Evaluation Experiment (Prichard  
819 et al., 2019; Liu et al., 2019) have started unravelling some of the unknowns associated with  
820 smoke plume chemistry and aerosol physics, however, work is still needed that integrates  
821 observations with existing modeling smoke models. For example, shading from smoke aerosols  
822 can limit O<sub>3</sub> production in smoke plume despite wildfires emitting chemical precursors that are  
823 conducive for O<sub>3</sub> production (Verma et al., 2009). There are also questions surrounding the  
824 timescale it takes for NO<sub>x</sub> to be converted into peroxyacetyl nitrate and then back to NO<sub>x</sub>, which  
825 can be used to form O<sub>3</sub> (Alvarado et al., 2010). These are just a few of the many questions that  
826 needs to be addressed regarding smoke plume chemistry.

827 Properly evaluating fire plume rise models also continues to be a challenging proposition.

828 There are a limited number of observational datasets that measure the plume height and  
829 properties, while simultaneously constraining surface fire characteristics, such as the fire heat  
830 flux, burned area, and fuel consumption. Incomplete observational datasets makes it difficult to  
831 disentangle whether a simulated plume rise result is erroneous due to assumptions made within  
832 the model, or if errors stem from the model inputs, *e.g.*, fire area and heat fluxes (Val Martin et  
833 al., 2012).

834 Finally, work is also needed to better project future fire behavior and emissions. Outside of  
835 coupled fire-atmosphere models, most smoke modeling frameworks either use a persistence  
836 assumption (smoke today will be the same as smoke yesterday) or scale current fire heat fluxes  
837 and emissions using a diurnal curve. Therefore, most smoke models are unable to account for  
838 weather-driven fire effects on the plume dynamics. Recent studies have indicated that climate  
839 change is now impacting how some fires behave during the nighttime (Chiodi et al., 2021),  
840 which could further limit the usefulness of diurnal scaling techniques. While running a coupled  
841 fire-atmosphere model for every wildfire may not be practical with today's computing resources,  
842 new approaches could be developed to project future fire intensity based forecasted weather  
843 conditions.

844 As we head further into the future, our ability to monitor fires will continue to improve as  
845 remote sensing products and their post-processing algorithms become more sophisticated. New  
846 and exciting new tools are emerging that synthesizes remote sensing products with machine  
847 learning techniques. These sorts of tools can provide detailed fire information at a high  
848 spatiotemporal resolution, therefore reducing some of the uncertainties described earlier in this  
849 chapter (Farguell et al., 2021). Such tools will be critical for providing accurate inputs into  
850 smoke modeling frameworks. It is expected that these emerging technologies, combined with

851 data assimilation and improved computational resources will play an increasingly important role  
852 towards improving the representation of smoke transport and dispersion within smoke model.

853

854

For Review Only

855  
856  
857  
858  
859  
860  
861  
862  
863  
864  
865  
866  
867  
868  
869  
870  
871  
872

## Figures and Tables:

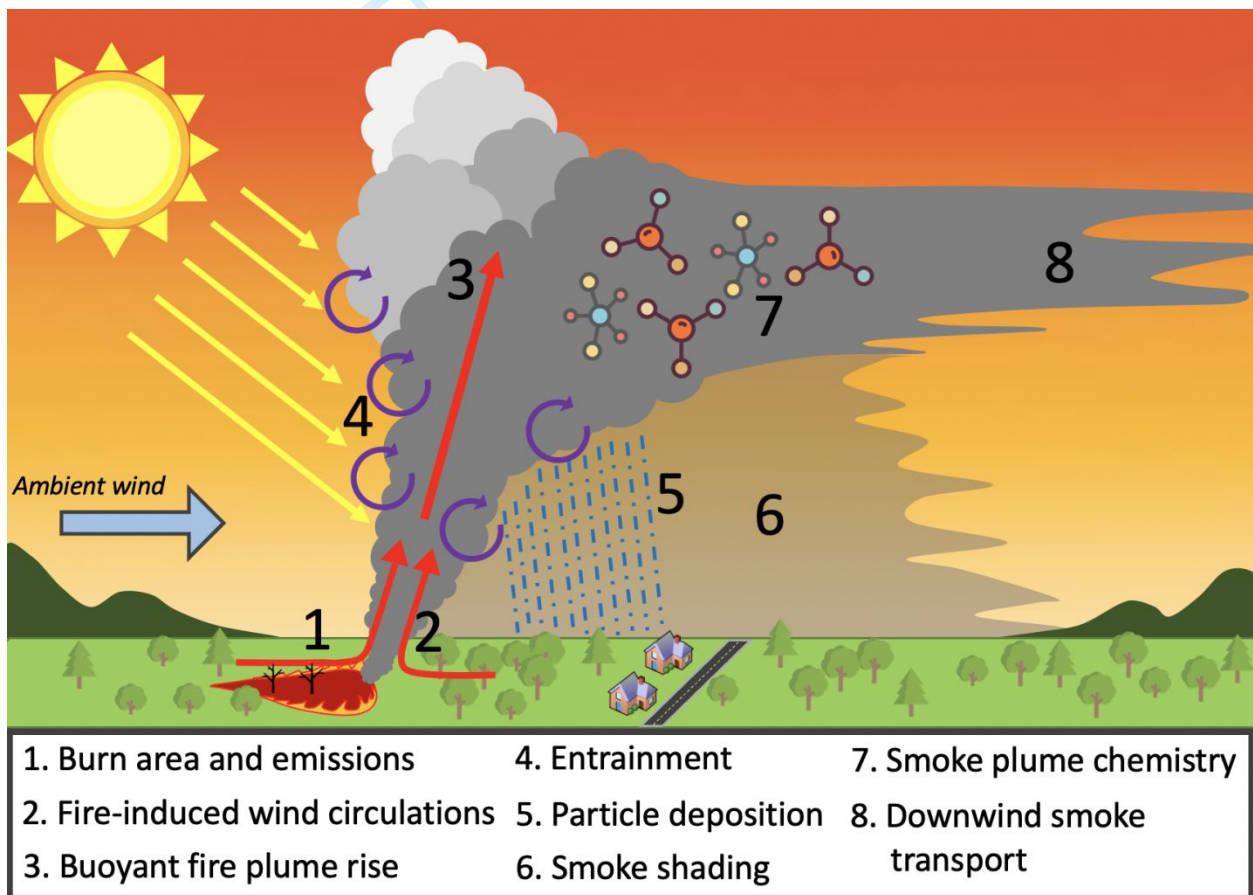
Table 1. List of commonly used smoke modeling frameworks for research and operational-based applications. The scale column are loose approximations of scales most appropriate for the listed model framework. Dashes within a column denote processes that are not accounted for. Gray shading intensity refers to the degree that specific processes are resolved where red is prescribed, yellow refers to processes that are parameterized, and green refers to explicitly resolve and/or parameterized and coupled.

Model	Model type	Scale	Fire Activity	Plume	Meteorology	Aerosol Physics	Chemistry
VSMOKE <sup>1</sup>	Gaussian	100-10,000m	Prescribed	Parameterized	Parameterized	-	Combustion only, smoke treated as passive tracer
SASEM <sup>2</sup>	Gaussian	100-10,000m	Prescribed	Parameterized	Parameterized	-	Combustion only, smoke treated as passive tracer
CALPUFF <sup>3</sup>	Puff model	1-1000 km	Prescribed	Parameterized	Parameterized	Parameterized	Parameterized
HYSPLIT <sup>4</sup>	Puff model	1-1000 km	Prescribed	Parameterized	Uncoupled	Parameterized	Parameterized
HYSPLIT <sup>4</sup>	LPDM	1-1000 km	Prescribed	Parameterized	Uncoupled	Parameterized	Parameterized
FLEXPART <sup>5</sup>	LPDM	1-1000 km	Prescribed	Parameterized	Uncoupled	Parameterized	Parameterized
STILT <sup>6</sup>	LPDM	1-1000 km	Prescribed	Parameterized	Uncoupled	Parameterized	Parameterized
DAYSMOKE <sup>7</sup>	Hybrid	1-10km	Parameterized	Parameterized	Parameterized or uncoupled	-	Combustion only, smoke treated as passive tracer
CMAQ-BlueSky <sup>8</sup>	Eularian	1-1000 km	Prescribed	Parameterized	Uncoupled	Parameterized	Parameterized
WRF-CHEM <sup>9</sup>	Eularian	1-1000 km	Prescribed	Parameterized	Resolved	Parameterized & coupled	Parameterized & coupled
GEOS-CHEM <sup>10</sup>	Eularian	"global"	Prescribed	Parameterized	Uncoupled	Parameterized	Parameterized
WRF-FIRE <sup>11</sup>	Coupled	100m-1000 km	Parameterized	Resolved	Resolved	-	Combustion only, smoke treated as passive tracer
WRF-SFIRE <sup>12</sup>	Coupled	100m-1000 km	Parameterized	Resolved	Resolved	Parameterized & coupled	Parameterized & coupled
WFDS <sup>13</sup>	Coupled	1m-1km	Resolved	Resolved	Resolved	-	Combustion only, smoke treated as passive tracer
HIGRAD-FIRETEC <sup>14</sup>	Coupled	1m-1km	Resolved	Resolved	Resolved	-	Combustion only, smoke treated as passive tracer

873  
874  
875  
876  
877  
878  
879  
880  
881  
882  
883

1. Lavdas (2006), 2. Sestak and Fiebau (1988), 3. Scire et al. (2000), 4. Draxler and Hess (1997), 5. Stohl and Thomson (1999), 6. Lin et al. (2003), 7. Achtemeir et al. (2011), 8. Larkin et al. (2009), 9. Grell et al. (2005), 10. <http://acmg.seas.harvard.edu/geos/>, 11. Coen et al. (2013), 12. Mandel et al. (2011), 13. Mell et al. (2007), 14. Linn and Cunningham (2005)

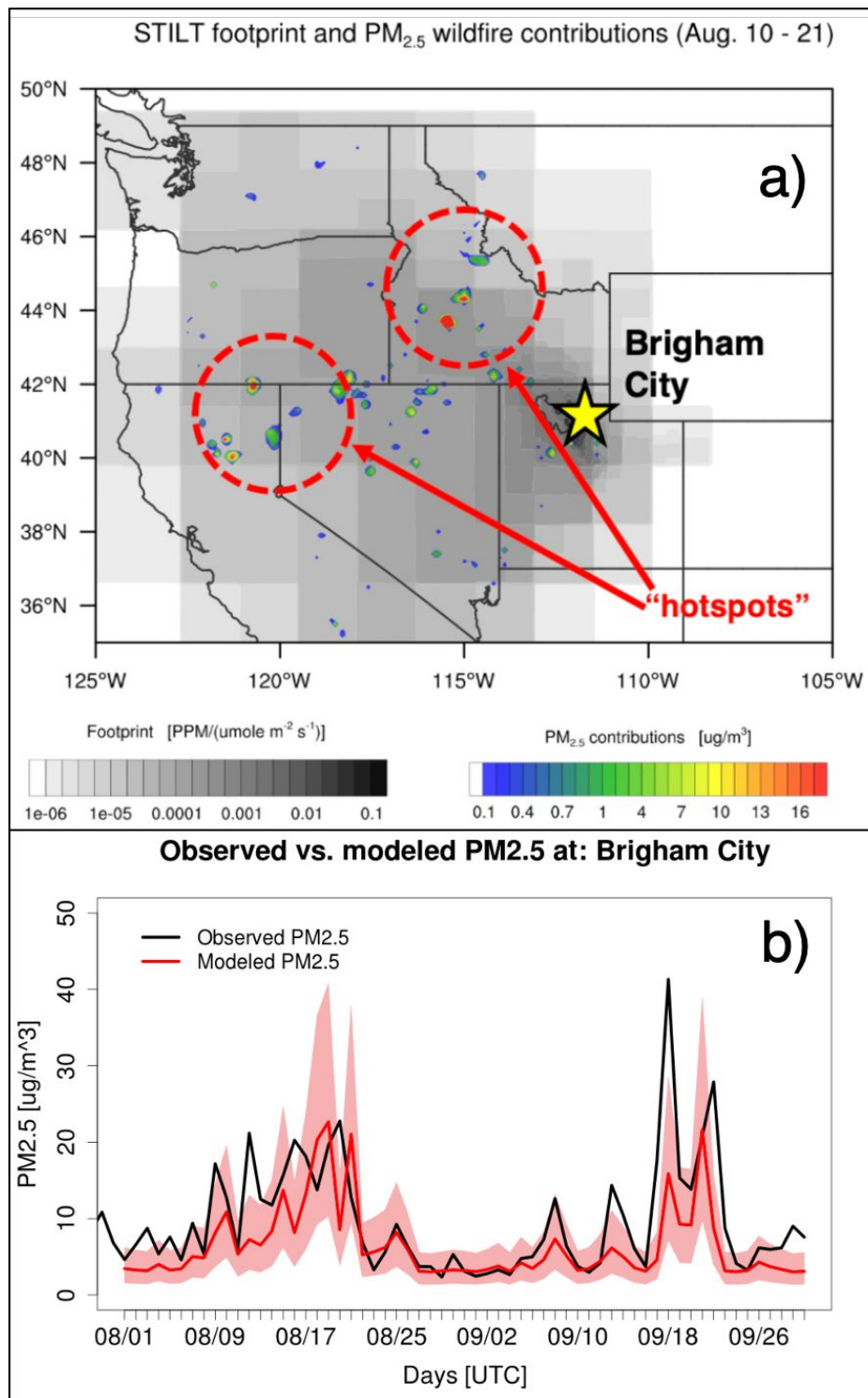
884  
885  
886  
887  
888  
889  
890  
891  
892  
893  
894  
895  
896  
897



898  
899  
900  
901  
902  
903  
904  
905  
906

Figure 1. A schematic of important smoke transport processes. Definitions and details of these processes can be found in the chapter text.

907



908

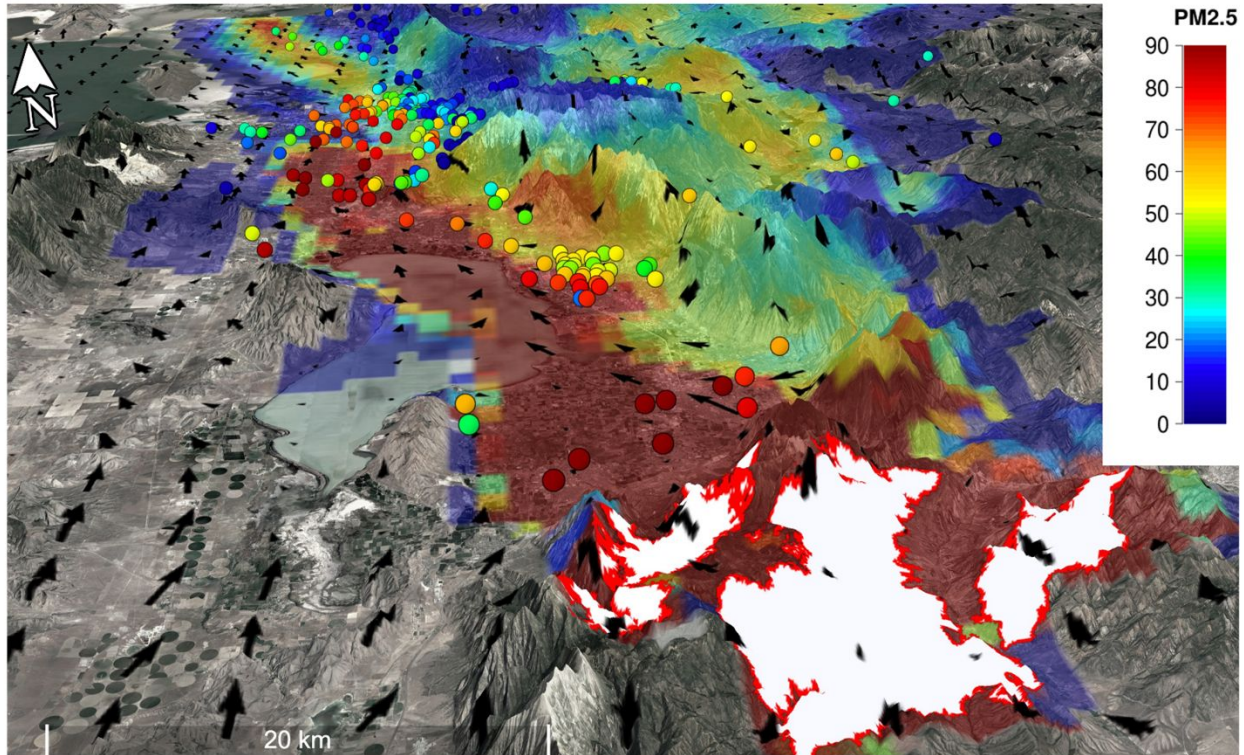
909 Figure 2. (a) STILT footprint (gray), which highlights backward trajectory transport pathways

910 averaged between August 10-21, 2012. PM<sub>2.5</sub> contributions from wildfires towards Brigham City911 are shown by the color-filled contours. (b) Observed vs. modeled PM<sub>2.5</sub> concentrations at

912 Brigham City, UT for an episodic smoke event (fall 2012) with model uncertainties (+/-1σ)

913 related to transport errors are shaded as pink.

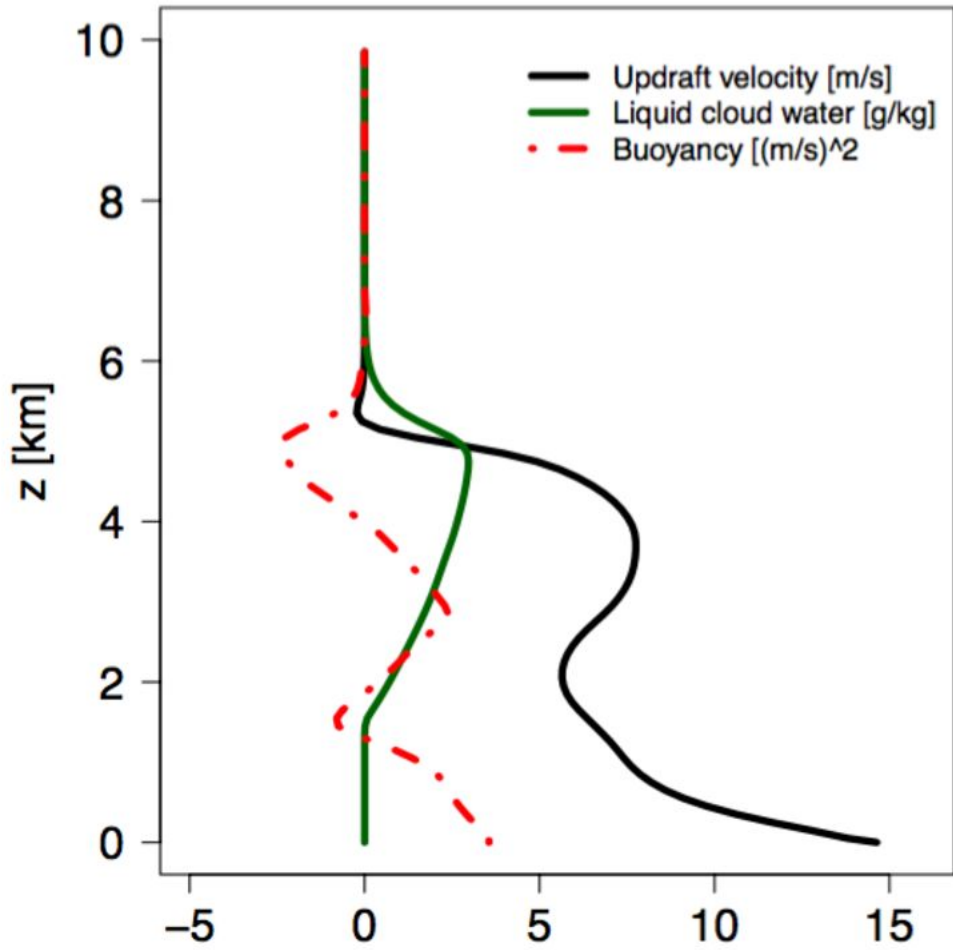
914  
915  
916  
917  
918  
919  
920



921  
922  
923  
924  
925  
926  
927  
928  
929  
930  
931  
932  
933  
934  
935  
936  
937  
938  
939  
940

Figure 3. WRF-SFIRE-simulated and observed PM<sub>2.5</sub> concentrations for the Pole Creek and Bald Mountain fire on September 15<sup>th</sup>, 2018. Simulated smoke concentrations are represented by the color-filled contours, while observed PM<sub>2.5</sub> concentrations are denoted by the color-filled circles. All PM<sub>2.5</sub> concentrations displayed here are in units of μg m<sup>-3</sup>. The white polygons in the lower right represent model-estimated burned areas, while the black arrows represent simulated near-surface winds.

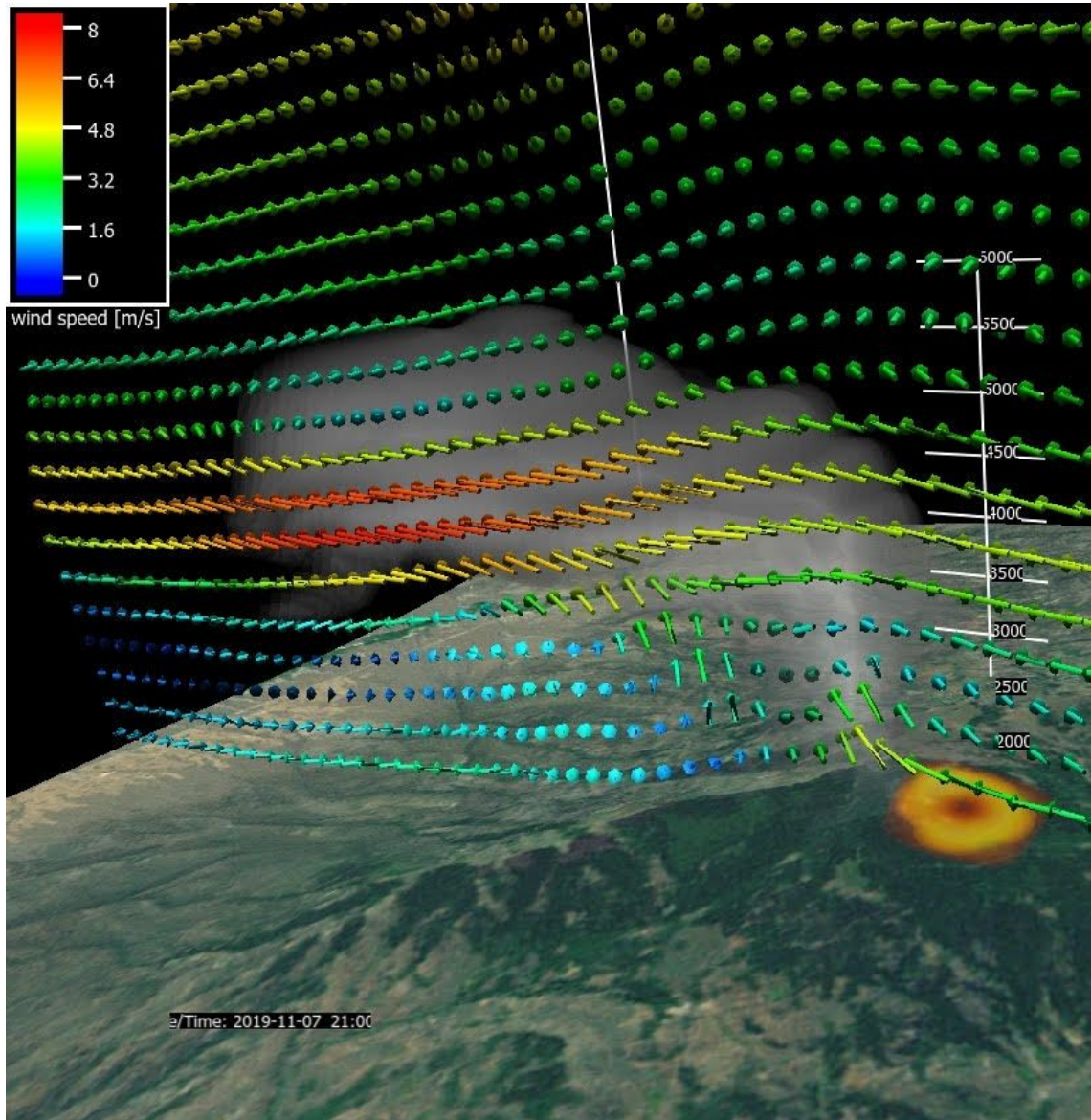
941  
942  
943  
944  
945  
946  
947



948  
949  
950  
951  
952  
953  
954  
955  
956  
957  
958  
959  
960  
961

Figure 4. Plume rise simulation generated from the Freitas plume model for the 2012 Dry Creek Fire in Alaska.

962  
963  
964  
965  
966  
967



968  
969  
970  
971  
972  
973  
974  
975  
976  
977

Figure 5. WRF-SFIRE simulated wildfire plume rise for the Anabella Reservoir prescribed burn. Warm-colored surface contours represent the modeled burn area, while the vectors represent simulated cross-sectional winds. Smoke is denoted by the transparent gray isosurface.

978 **References:**

- 979
- 980 Achtemeier, G. L., S. A. Goodrick, Y. Liu, F. Garcia-Menendez, Y. Hu, and M. T. Odman  
981 (2011), Modeling smoke plume rise and dispersion from southern United States prescribed burns  
982 with daysmoke. *Atmosphere*, 2, 358–388.
- 983
- 984 Ahmadov, R., G. Grell, E. James, S. Freitas, G. Pereira, I. Csiszar, et al. (2017). A  
985 high-resolution coupled meteorology-smoke modeling system HRRR-Smoke to simulate air  
986 quality over the CONUS domain in real time. *Geophysical Research Abstracts*, 19, 10841.
- 987
- 988 Akagi, S. K., R. J. Yokelson, C. Wiedinmyer, M. J. Alvarado, J. S. Reid, T. Karl, J. D. Crouse,  
989 and P. O. Wennberg (2011), Emission factors for open and domestic biomass burning for use in  
990 atmospheric models. *Atmos. Chem. Phys.*, 11, 4039–4072.
- 991
- 992 Alvarado, M. J. and Coauthors (2010), Nitrogen oxides and PAN in plumes from boreal fires  
993 during ARCTAS-B and their impact on ozone: an integrated analysis of aircraft and satellite  
994 observations. *Atmos. Chem. Phys.*, 10, 9739–9760.
- 995
- 996 Andreae, M.O., Merlet, P., 2001. Emission of trace gases and aerosols from biomass  
997 burning. *Glob. Biogeochem. Cycles*, 15, 955–966.
- 998
- 999 Andreae, M. O., D. Rosenfeld, P. Artaxo, A. A. Costa, G. P. Frank, K. M. Longo and M. A. F.  
1000 Silva-Dias (2004), Smoking rain clouds over the Amazon. *Science*, 303(5662), 1337–1342.
- 1001
- 1002 Archibald, A. T., M. E. Jenkin, and D. E. Shallcross (2010), An isoprene mechanism  
1003 intercomparison. *Atmos. Environ.*, 44, 5356–5364.
- 1004
- 1005 Baker, K., and Coauthors (2018), Photochemical model evaluation of 2013 California wild fire  
1006 air quality impacts using surface, aircraft, and satellite data. *Science of the Total Environment*,  
1007 637, 1137–1149.
- 1008
- 1009 Banta R. M., L. D. Olivier, E. T. Holloway, R. A. Kropfli, B. W. Bartram, R. E. Cupp, and M. J.  
1010 Post (1992), Smoke-column observations from two forest fires using Doppler lidar and Doppler  
1011 radar. *J. Applied Meteorology*, 31, 1328–1349.
- 1012
- 1013 Barnes, J. E. and D. J. Hofmann, (1997), Lidar measurements of stratospheric aerosol over  
1014 Mauna Loa Observatory. *Geophys. Res. Lett.*, 24, 1923–1926.
- 1015
- 1016 Battye, W., and R. Battye (2002), Final Report: Development of emissions inventory methods  
1017 for wildland fire. EPA. <https://www.epa.gov/ttn/chief/ap42/ch13/related/firerept.pdf>.
- 1018
- 1019 Bauer, S.E., and S. Menon (2012). Aerosol direct, indirect, semidirect, and surface albedo effects  
1020 from sector contributions based on the IPCC AR5 emissions for preindustrial and present-day  
1021 conditions. *J. Geophys. Res.*, 117, 1–15.
- 1022
- 1023 Bey, I., D. J. Jacob, R. M. Yantosca, J. A. Logan, B. D. Field, A. M. Fiore, and M. G. Schultz,

- 1024 (2001). Global modeling of tropospheric chemistry with assimilated meteorology: Model  
1025 description and evaluation. *J. Geophys. Res.*, 106(D19), 23073–23095.  
1026
- 1027 Brey, S. J., and E. V. Fischer (2016), Smoke in the city: How often and where does smoke  
1028 impact summertime ozone in the United States? *Environ. Sci. Technol.*, 50, 1288–94.  
1029
- 1030 Briggs, G. A. (1975), Plume Rise Predictions. Lectures on Air Pollution and Environmental  
1031 Impact Analyses. 72-73. *American Meteorological Society*, Boston, MA, USA.  
1032
- 1033 Brown J. K., L. S. Bradshaw (1994), Comparisons of particulate emissions and smoke impacts  
1034 from presettlement, full suppression, and prescribed natural fire periods in the Selway-Bitterroot  
1035 Wilderness. *International Journal of Wildland Fire*, 4(3), 143–155.  
1036
- 1037 Burling, I. R., R. J. Yokelson, D. W. T. Griffith, T. J. Johnson, P. Veres, J. M. Roberts, C.  
1038 Warneke, S. P. Urbanski, J. Reardon, J., D. R. Weise, W. M. Hao, W. M., and J. de Gouw,  
1039 (2010), Laboratory measurements of trace gas emissions from biomass burning of fuel types  
1040 from the southeastern and southwestern United States. *Atmos. Chem. Phys.*, 10, 1115–11130.  
1041
- 1042 Byun, D., and K. L. Schere (2006), Review of the governing equations, computational  
1043 algorithms, and other components of the Models-3 Community Multiscale Air Quality (CMAQ)  
1044 Modeling System. *Applied Mechanics Reviews*, 59, 51–77.  
1045
- 1046 Chen, L.-W. A., H. Moosmüller, W. P. Arnott, J. C. Chow, J. G. Watson, R. A. Susott, R.E.  
1047 Babbitt, C. E. Wold, E. N. Lincoln, W. M. Hao (2007), Emissions from laboratory combustion of  
1048 wildland fuels: emission factors and source profiles. *Environ. Sci. Technol.*, 2, 4317–4325.  
1049
- 1050 Chen, Y., Q. Li, J. T. Randerson, E. A. Lyons, R. A. Kahn, D. L. Nelson, and D. J. Diner (2009),  
1051 The sensitivity of CO and aerosol transport to the temporal and vertical distribution of North  
1052 American boreal fire emissions. *Atmos. Chem. Phys.*, 9, 6559–6580.  
1053
- 1054 Chin, M., R. B. Rood, S.-J. Lin, J. F. Muller, and A. M. Thompson (2000), Atmospheric sulfur  
1055 cycle in the global model GOCART: Model description and global properties, *J. Geophys. Res.*,  
1056 105, 24671–24687.  
1057
- 1058 Chiodi, A. M., B. E. Potter, and N. K. Larkin (2021), Multi-decadal change in Western US  
1059 nighttime vapor pressure deficit. *Geophys. Res. Lett.*, 48, e2021GL092830.  
1060
- 1061 Choi, Y-J, and H. J. S. Fernando (2007), Simulation of smoke plumes from agricultural burns:  
1062 application to the San Luis/Rio Colorado airshed along the US/Mexico border. *Sci. Total*  
1063 *Environ.*, 388(1–3), 270–289.  
1064
- 1065 Christian, K., J. Wang, C. Ge, D. Peterson, E. Hyer, J. Yorks, and M. McGill (2019), Radiative  
1066 forcing and stratospheric warming of pyrocumulonimbus smoke aerosols: First modeling results  
1067 with multisensor (EPIC, CALIPSO, and CATS) views from space. *Geophys. Res. Lett.*, 46,  
1068 10061–10071.  
1069

- 1070 Coen, J. L., M. Cameron, J. Michalakes, E. G. Patton, P. J. Riggan, and K. M. Yedinak (2013),  
1071 WRF-Fire: Coupled Weather -Wildland Fire Modeling with the Weather Research and  
1072 Forecasting Model. *J. Appl. Meteor. Climat.*, 52, 1, 16–38.  
1073
- 1074 Cunningham, P., S. L. Goodrick, M. Y. Hussaini, and R. R. Linn (2005), Coherent vortical  
1075 structures in numerical simulations of buoyant plumes from wildland fires. *International Journal*  
1076 *of Wildland Fire*, 14, 61–75.  
1077
- 1078 Cunningham, P., and S. L. Goodrick (2012), High-Resolution numerical models for  
1079 smoke transport in plumes from wildland fires. *Remote Sensing and Modeling Applications to*  
1080 *Wildland Fires*. Springer-Verlag, Tsinghua University Press, pp. 74–88.  
1081
- 1082 Decker, Z. C., and Coauthors (2021), Nighttime and daytime dark Oxidation Chemistry in  
1083 Wildfire Plumes: An Observation and Model Analysis of FIREX-AQ Aircraft Data, *Atmos.*  
1084 *Chem. Phys. Discuss.*, <https://doi.org/10.5194/acp-2021-267>.  
1085
- 1086 Draxler, R. R., and G. D. Hess (1997), Description of the HYSPLIT\_4 modeling system. NOAA  
1087 Technical Memorandum ERL, ARL-224.  
1088
- 1089 Elguindi, N., H. Clark, C. Ordóñez, V. Thouret, J. Flemming, O. Stein, V. Huijnen, P. Moinat, A.  
1090 Inness, V.-H. Peuch, A. Stohl, S. Turquety, G. Athier, J.-P. Cammas, and M. Schultz (2020),  
1091 Current status of the ability of the GEMS/MACC models to reproduce the tropospheric CO  
1092 vertical distribution as measured by MOZAIC. *Geosci. Model Dev.*, 3, 501–518.  
1093
- 1094 Emerson, E. W., A. L. Hodshire, H. M. DeBolt, K. R. Bilback, J. R. Pierce, G. R. McMeeking,  
1095 and D. K. Farmer (2020), Revisiting particle dry deposition and its role in radiative effect  
1096 estimates. *PNAS*, 117(42), 26076–26082.  
1097
- 1098 Emmons, L. K., and Coauthors (2010), Description and evaluation of the model for ozone and  
1099 related chemical tracers, version 4 (MOZART-4). *Geosci. Model Dev.*, 3(1), 43–67.  
1100
- 1101
- 1102 Farguell, A., J. Mandel, J. Haley, D. V. Mallia, A. Kochanski, and K. Hillburn (2021), Machine  
1103 learning estimation of fire arrival time from level-2 active fire satellite data. *Remote Sensing*,  
1104 13(11), 2203.  
1105
- 1106 Finlayson-Pitts, B.J., and J. N. Pitts, (1986), *Atmospheric Chemistry: Fundamentals and*  
1107 *Experimental Techniques*. John Wiley and Sons, New York, NY.  
1108
- 1109 Forrister, H., J. Liu, E. Scheuer, J. Dibb, L. Ziemba, K. L. Thornhill, et al. (2015). Evolution of  
1110 brown carbon in wildfire plumes. *Geophys. Res. Lett.*, 42, 4623–4630.  
1111
- 1112 Freitas, S. R., K. M. Longo, R. Chatfield, D. Latham, M. A. F. S. Dias, M. O. Andreae, E. Prins,  
1113 J. C. Santos, R. Gielow, and J. A. Carvalho (2007), Including the sub-grid scale plume rise of  
1114 vegetation fires in low resolution atmospheric transport models. *Atmos. Chem. Phys.*, 7, 3385–  
1115 3398.

- 1116  
1117 Freitas, S. R., K. M. Longo, J. Trentmann, and D. Latham (2010), Technical note: Sensitivity of  
1118 1-D smoke plume rise models to the inclusion of environmental wind drag. *Atmos. Chem. Phys.*,  
1119 10, 585–594.  
1120  
1121 Fromm, M., D. T. Lindsey, R. Servranckx, G. Yue, T. Trickl, R. Sica, P. Doucet, and S. Godin-  
1122 Beekmann (2010), The untold story of the pyrocumulonimbus. *BAMS*, 91(9), 1193–1210.  
1123  
1124 Giglio, L. (2007), Characterization of the tropical diurnal fire cycle using VIRS and MODIS  
1125 observations. *Remote Sens. Environ.*, 108(4), 407–421.  
1126  
1127 Goodrick, S. L., G. L. Achtemeier, N. K. Larkin, Narasimhan, Y. Liu, T. Strand (2012),  
1128 Modelling smoke transport from wildland fires: a review, *Int. J. Wildland Fire*,  
1129 <http://dx.doi.org/10.1071/WF11116>.  
1130  
1131 Grell G. A., S. E. Peckham, S. McKeen, R. Schmitz, G. Frost, W. C. Skamarock, and B. Eder  
1132 (2005), Fully coupled ‘online’ chemistry within the WRF model. *Atmospheric Environment*, 39,  
1133 6957–6975.  
1134  
1135 Grell, G., S. R. Freitas, M. Stuefer, and J. Fast (2011), Inclusion of biomass burning in WRF-  
1136 Chem: impact of wildfires on weather forecasts. *Atmos. Chem. Phys. Discuss.*, 10, 30 613–30  
1137 650.  
1138  
1139 Hodzic, A., S. Madronich, B. Bohn, S. Massie, L. Menut and C. Wiedinmyer (2007), Wildfire  
1140 particulate matter in Europe during summer 2003: meso-scale modeling of smoke emissions,  
1141 transport and radiative effects. *Atmos. Chem. Phys. Discuss.*, 7(2), 4705–4760.  
1142  
1143 Haikerwal, A., F. Reisen, M. R. Sim, M. J. Abramson, C. P. Meyer, F. H. Johnston, and M.  
1144 Dennekamp (2015), Impact of smoke from prescribed burning: Is it a public health concern? *J.*  
1145 *Air and Waste Manage. Assoc.*, 65, 592–598.  
1146  
1147 Hyer, E. J. and B. N. Chew (2010), Aerosol transport model evaluation of an extreme smoke  
1148 episode in Southeast Asia. *Atmos. Environ.*, 44, 1422–1427.  
1149  
1150 Jackson W. A., G. L. Achtemeier, and S. L. Goodrick (2007); A technical evaluation of smoke  
1151 dispersion from the Brush Creek Prescribed fire and the impacts on Asheville, North Carolina.  
1152 Available at:  
1153 [http://www.nifc.gov/smoke/documents/Smoke\\_Incident\\_Impacts\\_Ashville\\_NC.pdf](http://www.nifc.gov/smoke/documents/Smoke_Incident_Impacts_Ashville_NC.pdf).  
1154  
1155 Jaffe, D., I. Bertschi, L. Jaegle, P. Novelli, J. S. Reid, H. Tanimoto, R. Vingarzan, and D. L.  
1156 Westphal (2004), Long-range transport of Siberian biomass burning emissions and impact on  
1157 surface ozone in western North America. *Geophys. Res. Lett.*, 31, L16106.  
1158  
1159 Jaffe, D. A., and N. L. Wigder (2012), Ozone production from wildfires: A critical review.  
1160 *Atmos. Environ.*, 51, 1–10.  
1161

- 1162 Jain R, J. Vaughan, H. Kyle, C. Ramosa, C. Clalborn, S. Maarten, M. Schaaf, and B. Lamb  
1163 (2007), Development of the ClearSky smoke dispersion forecast system for agricultural field  
1164 burning in the Pacific Northwest. *Atmos. Environ.*, 41, 6745–6761.  
1165
- 1166 Kalnay, E. (2003), *Atmospheric Modeling, Data Assimilation and Predictability*. Cambridge  
1167 University Press, 369 pp.  
1168
- 1169 Kochanski, A. K., M. A. Jenkins, K. Yedinak, J. Mandel, J. Beezley, and B. Lamb (2016),  
1170 Toward an integrated system for fire, smoke, and air quality simulations, *Int. J. Wildland*  
1171 *Fire*, 25, 558–568.  
1172
- 1173 Kochanski, A. K., A. Fournier, and J. Mandel (2018), Experimental design of a prescribed burn  
1174 instrumentation. *Atmosphere*, 9, 296.  
1175
- 1176 Kochanski, A. K., D. V. Mallia, M. Fearon, T. Brown, and J. Mandel (2019), Modeling wildfire  
1177 smoke feedback mechanisms using a coupled fire-atmosphere model with a radiatively active  
1178 aerosol scheme. *J. Geophys. Res.*, 124(16), 9099–9116.  
1179
- 1180 Lahm, P. (2015), Wildfire, prescribed fire and the Clean Air Act: the latest challenges and  
1181 opportunities. *6th International Fire Ecology and Management Congress: advancing ecology in*  
1182 *fire management*, November 16–20, San Antonio, TX.  
1183
- 1184 Latham, D. (1994), PLUMP: A one-dimensional plume predictor and cloud model for fire and  
1185 smoke managers. *Gen. Tech. Rep. INT-GTR-314*, Intermt. Res. Stn., For. Serv., U.S. Dep. of  
1186 Agric., Fort Collins, Colo  
1187
- 1188 Lavdas, L. G. (1996), Program VSMOKE – users manual. USDA Forest Service, Southeastern  
1189 Forest Experiment Station, General Technical Report SRS-6. (Macon GA)  
1190
- 1191 Lareau, N. P. and C. B. Clements (2015), Cold Smoke: smoke-induced density currents cause  
1192 unexpected smoke transport near large wildfires, *Atmos. Chem. Phys.*, 15, 11513–11520.  
1193
- 1194 Lareau, N. P. and C. B. Clements (2016), Environmental controls on pyrocumulus and  
1195 pyrocumulonimbus initiation and development. *Atmos. Chem. Phys.*, 16, 4005–4022.  
1196
- 1197 Lareau, N., and C. Clements, 2017: The mean and turbulent properties of a wildfire convective  
1198 plume. *J. Appl. Meteor. Climatol.*, 56(8), 2289–2299.  
1199
- 1200 Larkin, N. K., S. M. O'Neill, R. Solomon, S. Raffuse, T. Strand, D. C. Sullivan, and S. A.  
1201 Ferguson (2009), The BlueSky Smoke Modeling Framework. *Int. J. Wildland Fire*, 18, 906–920.  
1202
- 1203 Lee, H., S.-J. Jeong, O. Kalashnikova, M. Tosca, S.-W. Kim, and J.-S. Kug, (2018),  
1204 Characterization of wildfire-induced aerosol emissions from the Maritime Continent peatland  
1205 and Central African dry savannah with MISR and CALIPSO aerosol products. *J. Geophys. Res.*,  
1206 123, 3116–3125.  
1207

- 1208 Lelieveld, J., J. S. Evans, M. Fnais, D. Giannadaki, and A. Pozzer (2015), The contribution of  
1209 outdoor air pollution sources to premature mortality on a global scale. *Nature*, 525, 367–384.  
1210
- 1211 Leung, F.-Y. T., J. A. Logan, R. Park, E. Hyer, E. Kasischke, D. Streets, and L. Yurganov  
1212 (2007), Impacts of enhanced biomass burning in the boreal forests in 1998 on tropospheric  
1213 chemistry and the sensitivity of model results to the injection height of emissions. *J. Geophys.  
1214 Res.-Atmos.*, 112, D10313.  
1215
- 1216 Li, Y., M. J. Loretta, P. Liu, and J. O. Kaplan (2020), Trends and spatial shifts in lightning fires  
1217 and smoke concentrations in response to 21st century climate over the national forests and parks  
1218 of the western United States. *Atmos. Phys. Chem.*, 20, 8827–8838.  
1219
- 1220 Lim, C. Y., and Coauthors (2019), Secondary organic aerosol formation from the laboratory  
1221 oxidation of biomass burning emissions. *Atmos. Chem. Phys.*, 19, 12797–12809.  
1222
- 1223 Lindsey, D. T., and M. Fromm (2008), Evidence of the cloud lifetime effect from  
1224 wildfire-induced thunderstorms. *Geophys Res. Lett.*, 35, L22809.  
1225
- 1226 Linn R. R., J. Reisner, J. J. Colmann, and J. Winterkamp (2002), Studying wildfire behavior  
1227 using FIRETEC. *Int. J. Wildland Fire*, 11, 233–246.  
1228
- 1229 Linn, R. R., and P. Cunningham (2005), Numerical simulations of grass fires using a coupled  
1230 atmosphere-fire model: basic fire behavior and dependence on wind speed. *J Geophys. Res.*, 110,  
1231 D13107.  
1232
- 1233 Liu, X., P.-L. Ma, H. Wang, S. Tilmes, B. Singh, R. C. Easter, S. J. Ghan, and P. J. Rasch  
1234 (2016b), Description and evaluation of a new 4-mode version of Modal Aerosol Module  
1235 (MAM4) within version 5.3 of the Community Atmosphere Model. *Geosci. Model. Dev.*, 9, 505–  
1236 522.  
1237
- 1238 Liu, Y., S. Goodrick, G. Achtemeier, W. Jackson, J. Qu, and W. Wang (2009), Smoke incursions  
1239 into an urban area: simulation of a Georgia prescribed burn. *Int. J. Wildland Fire*, 18(3), 336–  
1240 348.  
1241
- 1242 Liu, Y. Q., G. L. Achtemeier, S. L. Goodrick, and W. A. Jackson (2010), Important parameters  
1243 for smoke plume rise simulation with Daysmoke. *Atmospheric Pollution Research*, 1, 250–259.  
1244
- 1245 Liu, J. C., and Coauthors (2016a), Particulate air pollution from wildfires in the Western U.S.  
1246 under climate change. *Climate Change*, 138, 655–666.  
1247
- 1248 Liu Y., A. Kochanski, K. Baker, W. Mell, R. Linn, R. Paugam, J. Mandel, A. Fournier, M.  
1249 Jenkins, S. Goodrick, G. Achtemeier, F. Zhao, R. Ottmar, N. French, N. Larkin, T. Brown, A.  
1250 Hudak, M. Dickinson, B. Potter, C. Clements, S. P. Urbanski, S. Prichard, A. Watts, and D.  
1251 McNamara (2019), Fire behavior and smoke modelling: model improvement and measurement  
1252 needs for next-generation smoke research and forecasting systems. *International Journal of  
1253 Wildland Fire* 28, 570-588.

- 1254  
1255 Lobert, J. (1991), Experimental evaluation of biomass burning emissions: nitrogen and carbon  
1256 containing compounds, in: *Global Biomass Burning: Atmospheric, Climatic and Biospheric*  
1257 *Implications*. MIT Press, Cambridge, MA, pp. 289–304.  
1258
- 1259 Loughner, C., B. Fasoli, A.F. Stein, and J.C. Lin (2021), Incorporating features from the  
1260 Stochastic Time-Inverted Lagrangian Transport (STILT) model into the Hybrid Single-Particle  
1261 Lagrangian Integrated Trajectory (HYSPLIT) model: a unified dispersion model for time-  
1262 forward and time-reversed applications, *J. Appl. Meteor. Climat.*, 60, 799–810.  
1263
- 1264 Lu, Z., and I. N. Sokolik (2013), The effect of smoke emission amount on changes in cloud  
1265 properties and precipitation: A case study of Canadian boreal wildfires of 2007. *J. Geophys.*  
1266 *Res.*, 118, 11777–11793.  
1267
- 1268 Luderer, G., J. Trentmann, T. Winterrath, C. Textor, M. Herzog, H.-F. Graf, and M. O. Andreae  
1269 (2006), Modeling of biomass smoke injection into the lower stratosphere by a large forest fire  
1270 (Part II): sensitivity studies. *Atmos. Chem. Phys.* 6, 5261–5277.  
1271
- 1272 Mallia, D. V., J. C. Lin, S. Urbanski, J. Ehleringer, and T. Nehr Korn (2015), Impacts of upwind  
1273 wildfire emissions on CO<sub>2</sub>, CO, and PM<sub>2.5</sub> concentrations in Salt Lake City, Utah. *J. Geophys.*  
1274 *Res.*, 120(1), 147–166.  
1275
- 1276 Mallia, D. V., A. Kochanski, S. Urbanski, and J. C. Lin (2018), Optimizing smoke and plume  
1277 rise modeling approaches at local scales. *Atmosphere*, 9, 116.  
1278
- 1279 Mallia, D. V., A. Kochanski, S. Urbanski, J. Mandel, A. Farguell, and S. Krueger (2020a),  
1280 Incorporating a canopy parameterization within a coupled fire-atmosphere model to improve a  
1281 smoke simulation for a prescribed burn. *Atmosphere*, 11(8), 832.  
1282
- 1283 Mallia, D. V., A. K. Kochanski, K. E. Kelly, R. Whitaker, W. Xing, L. Mitchell, A. Jacques, A.  
1284 Farguell, J. Mandel, P.-E. Gaillardon, T. Becnel, and S. Krueger (2020b), Evaluating wildfire  
1285 smoke transport within a coupled fire-atmosphere model using a high-density observation  
1286 network for an episodic smoke event along Utah’s Wasatch Front. *J. Geophys. Res.*, 125,  
1287 e2020JD032712.  
1288
- 1289 Mandel, J., J. D. Beezley, A. K. Kochanski (2011), Coupled atmosphere-wildland fire modeling  
1290 with WRF 3.3 and SFIRE 2011. *Geosci. Model Devel.*, 4, 591–610.  
1291
- 1292 McMeeking G. R., S. M. Kreidenweis, S. Baker, C. M. Carrico, J. C. Chow, J. L. Collett, W. M.  
1293 Hao, A. S. Holden, T. W. Kirchstetter, W.C. Malm, H. Moosmüller, A. P. Sullivan, C. E. Wold (2009),  
1294 Emissions of trace gases and aerosols during the open combustion of biomass in the  
1295 laboratory. *J. Geophys. Res.-Atmos.*, 114, D19210.  
1296
- 1297 Mell, W., M. A. Jenkins, J. Gould, and P. Cheney P (2007), A physics-based approach to  
1298 modeling grassland fires. *Int. J. Wildland Fire*, 16, 1–22.  
1299

- 1300 O'Neill, S.M., N. K Larkin, J. Hoadley, G. Mills, J. Vaughan, R. Draxler, G. Roph, M.  
1301 Ruminski, and S. A. Ferguson (2008), Regional real-time smoke prediction systems. *Wildland*  
1302 *Fires and Air Pollution*, A. Bytnerowicz et al., Eds., *Developments in Environmental Science*  
1303 *Series*, Vol. 8, Elsevier, 499-534.
- 1304  
1305 Paugam, R., M. Wooster, S. Freitas, and M. Val Martin (2016), A review of approaches to  
1306 estimate wildfire plume injection height within large-scale atmospheric chemical transport  
1307 model. *Atmos. Chem. Phys.*, 16, 907–925.
- 1308  
1309 Paulot, F., J. D. Crouse, H. G. Kjaergaard, J. H. Kroll, J. H. Seinfeld, and P. O. Wennberg  
1310 (2009), Isoprene photooxidation: new insights into the production of acids and organic nitrates.  
1311 *Atmos. Chem. Phys.*, 9, 1479–1501.
- 1312  
1313 Peng, Q., and Coauthors (2020), HONO emissions from western U.S. wildfires provide dominant  
1314 Radical source in fresh wildfire smoke. *Environ. Sci. Technol.*, 54(10), 5954–5963.
- 1315  
1316 Peterson, D. A., J. R. Campbell, E. J. Hyer, M. D. Fromm, G. P. Kablick, J. H. Cossuth, and M.  
1317 T. DeLand (2018), Wildfire-driven thunderstorms cause a volcano-like stratospheric injection of  
1318 smoke. *npj Climate and Atmospheric Science*, 1(1), 30.
- 1319  
1320 Peterson, J. and Coauthors (2020), NWCG Smoke Management Guide for Prescribed Fire.  
1321 *National Wildfire Coordinating Group*. PMS 420-3.
- 1322  
1323 Pfister, G. G., C. Wiedinmyer, and L. K. Emmons (2008), Impacts of the fall 2007 California  
1324 wildfires on surface ozone: Integrating local observations with global model simulations.  
1325 *Geophys. Res. Lett.*, 35.
- 1326  
1327 Pfister, G. G., J. Avise, C. Wiedinmyer, D. P. Edwards, L. K. Emmons, G. D. Diskin, J.  
1328 Podolske, and A. Wisthaler (2011), CO source contribution analysis for California during  
1329 ARCTAS-CARB. *Atmos. Chem. Phys.*, 11(15), 7515–7532.
- 1330  
1331 Pharo J. A., L. G. Lavdas and P. M. Bailey PM (1976), Smoke Transport and Dispersion. In  
1332 'Southern Forestry and Smoke Management Guidebook'. (Ed. HE Mobley) USDA Forest  
1333 Service, Southeastern Research Station, General Technical Report SE-10, Chap. 5, pp. 45–55.
- 1334  
1335 Powers, J., and Coauthors (2017), The Weather Research and Forecasting Model: Overview,  
1336 system efforts, and future direction. *Bull. Amer. Meteor.*, 98(8), 1717–1737.
- 1337  
1338 Prichard, S. and Coauthors (2019), The fire and smoke model evaluation experiment—a plan for  
1339 integrated, large fire–atmosphere field campaigns. *Atmosphere*, 10(2), 66.
- 1340  
1341 Raffuse, S. M., K. J. Craig, N. K. Larkin, T. T. Strand, D. C. Sullivan, N. J. M. Wheeler, and R.  
1342 Solomon (2012), An Evaluation of modeled plume injection height with satellite-derived  
1343 observed plume height. *Atmosphere*, 3, 103–123.
- 1344  
1345 Rappold, A. G., N. L. Fann, J. Crooks, J. Huang, W. E. Cascio, R. B. Devlin, D. Diaz-Sanchez

- 1346 (2014), Forecast-based interventions can reduce the health and economic burden of wildfires.  
1347 *Environ. Sci. & Technol.*, 48(8), 10571–10579.
- 1348
- 1349 Robock, A. (1988), Enhancement of Surface Cooling Due to Forest Fire Smoke, *Science*, 242,  
1350 911–913.
- 1351
- 1352 Robock, A. (1991), Surface cooling due to forest fire smoke, *J. Geophys. Res.*, 96, 2156–2202.
- 1353
- 1354 Robock, A. (2000), Volcanic eruptions and climate. *Rev. Geophys.*, 38, 191–219.
- 1355
- 1356 Rothermel R (1972), A mathematical model for predicting fire spread in wildland fuels.  
1357 Technical Report Research Paper INT 115, USDA Forest Service, Intermountain Forest and  
1358 Range Experiment Station, Ogden, UT, 1-46.
- 1359
- 1360 Saylor, R. D., D. Barry, P. Lee, D. Tong, L. Pan and B. B. Hicks (2019), The particle dry  
1361 deposition component of total deposition from air quality models: right, wrong or uncertain?  
1362 *Tellus B: Chemical and Physical Meteorology*, 71:1, 1550324.
- 1363
- 1364 Scire, J. S., D. G. Strimaitis, and R. J. Yamartino (2000), A user's guide for the CALPUFF  
1365 Dispersion Model (version 5.0). edited, pp. 521-521, Earth Tech, Inc, Concord, MA.
- 1366
- 1367 Segal, M. and R. W. Arritt (1992), Nonclassical mesoscale circulations caused by surface  
1368 sensible heat-flux gradients, *B. Am. Meteor. Soc.*, 73, 1593–1604.
- 1369
- 1370 Sessions, W. R., H. E. Fuelberg, R. A. Kahn, and D. M. Winker (2011), An investigation of  
1371 methods for injecting emissions from boreal wildfires using WRF-Chem during ARCTAS.  
1372 *Atmos. Chem. Phys.*, 11(12), 5719–5744.
- 1373
- 1374 Sestak, M. L. and A. R. Riebau (1988), SASEM, Simple approach smoke estimation model. US  
1375 Bureau of Land Management, Technical Note 382.
- 1376
- 1377 Shin, H. H., and S.-Y. Hong (2015), Representation of the subgrid-scale turbulent transport in  
1378 convective boundary layers at gray-zone resolutions. *Mon. Wea. Rev.*, 143, 250–271.
- 1379
- 1380 Sofiev, M., T. Ermakova, and R. Vankevich (2012), Evaluation of the smoke-injection height  
1381 from wild-land fires using remote-sensing data. *Atmos. Chem. Phys.*, 12, 1995–2006.
- 1382
- 1383 Sofiev, M., R. Vankevich, T. Ermakova, and J. Hakkarainen (2013), Global mapping of  
1384 maximum emission heights and resulting vertical profiles of wildfire emissions. *Atmos. Chem.*  
1385 *Phys.*, 13, 7039–7052.
- 1386
- 1387 Spracklen, D. V., L. J. Mickley, J. A. Logan, R. C. Hudman, R. Yevich, M. D. Flannigan, and A.  
1388 L. Westerling (2009), Impacts of climate change from 2000 to 2050 on wildfire activity and  
1389 carbonaceous aerosol concentrations in the western United States. *J. Geophys. Res.*, 114,  
1390 D20301.
- 1391

- 1392 Solomos, S., V. Amiridis, P. Zanis, E. Gerasopoulos, F. I. Sofiou, T. Herekakis, J. Brioude, A.  
1393 Stohl, R. Kahn, and C. Kontoes (2015), Smoke dispersion modeling over complex terrain using  
1394 high resolution meteorological data and satellite observations - The Fire Hub platform, *Atmos.*  
1395 *Environ.*, 119, 348–361.
- 1396  
1397 Taylor, G. I. (1922), Diffusion by continuous movements. *Proc. London Math. Soc.*, 20, 196–  
1398 212.
- 1399  
1400 Tanimoto, H., K. Matsumoto, M. Uematsu, (2008), Ozone-CO correlations in Siberian wildfire  
1401 plumes observed at Rishiri Island. *Sola*, 4, 65–68.
- 1402  
1403 Trentmann, J., G. Luderer, T. Winterrath, M. D. Fromm, R. Servranckx C. Textor  
1404 M. Herzog G.-F. Graf, and M. O Andreae (2006), Modeling of biomass smoke injection into the  
1405 lower stratosphere by a large forest fire (Part I): reference simulation. *Atmos. Chem. Phys.*, 6,  
1406 5247–5260.
- 1407  
1408 Turquety, S., J. A. Logan, D. J. Jacob, R. C. Hudman, F. Y. Leung, C. L. Heald, R. M. Yantosca,  
1409 D. Wu, L. K. Emmons, D. P. Edwards, and G. W. Sachse (2007), Inventory of boreal fire  
1410 emissions for North America in 2004: Importance of peat burning and pyroconvective injection.  
1411 *J. Geophys. Res.-Atmos.*, 112, D12S03.
- 1412  
1413 Urbanski, S. P., W. M. Hao, and B. Nordgren (2011), The wildland fire emission inventory:  
1414 western United States emission estimates and an evaluation of uncertainty. *Atmos. Chem. Phys.*,  
1415 11, 12973–1300.
- 1416  
1417 Urbanski, S. (2014), Wildland fire emissions, carbon, and climate: Emission factors. *Forest Ecol.*  
1418 *Manage.*, 317, 51–60.
- 1419  
1420 Urbanski, S. P., M. C. Reeves, R. E. Corley, W. M. Hao, and R. P. Silverstein (2017), Missoula  
1421 Fire Lab Emission Inventory (MFLEI) for CONUS. Fort Collins, CO: Forest Service Research  
1422 Data Archive. <https://doi.org/10.2737/RDS-2017-0039>
- 1423  
1424 Val Martin, N., R. Kahn, J. A. Logan, R. Pausnam, M. Wooster, and C. Ichoku (2012), Space-  
1425 based observational constraints for 1-D fire smoke plume-rise models. *J. Geophys. Res.*, 117,  
1426 D22204.
- 1427  
1428 van der Werf, G. R., J. T. Randerson, L. Giglio, G. J. Collatz, M. Mu, P. S. Kasibhatla and T. T.  
1429 v. Leeuwen (2010), Global fire emissions and the contribution of deforestation, savanna, forest,  
1430 agricultural, and peat fires (1997–2009). *Atmos. Chem. Phys.*, 10(23), 11707–11735.
- 1431  
1432 Walcek, C. J. (2002), Effects of wind shear on pollution dispersion. *Atmos. Environ.*, 36, 511–  
1433 517.
- 1434  
1435 Walter, C., S. R. Freitas, C. Kottmeier, I. Kraut, D. Rieger, H. Vogel, and B. Vogel (2016), The  
1436 importance of plume rise on the concentrations and atmospheric impacts of biomass burning  
1437 aerosol. *Atmos. Chem. Phys.*, 16(14), 9201–9219.

- 1438  
1439 Wiedinmyer, C., S. K. Akagi, R. J. Yokelson, L. K. Emmons, J. A. Al-Saadi, J. J. Orlando, A. J.  
1440 Soja (2010), The Fire INventory from NCAR (FINN): a high resolution global model to estimate  
1441 the emissions from open burning. *Geosci. Model Develop. Discuss.*, 3, 2439–2476.  
1442  
1443 Weisman, M. L., C. Davis, W. Wang, K. W. Manning, and J. B. Klemp (2008), Experiences with  
1444 0–36-h explicit convective forecasts with the WRF-ARW Model. *Wea. Forecasting*, 23, 407–  
1445 437.  
1446  
1447 Westerling, A. L., H. G. Hidalgo, D. R. Cayan, and T. W. Swetnam (2006), Warming and earlier  
1448 spring increases western U.S. forest fire activity. *Science*, 313, 940–943.  
1449  
1450 Wolfe, G. M., M. R. Marvin, S. J. Roberts, K. R. Travis and J. Liao (2016), The framework for  
1451 0-D atmospheric modeling (F0AM) v3.1, *Geosci. Model Dev.*, 9(9), 3309–3319.  
1452  
1453 Wotawa, G., M. Trainer (2000), The influence of Canadian forest fires on pollutant  
1454 concentrations in the United States. *Science*, 288, 324–328.  
1455  
1456 Xie, M., M. D. Hays, and A. L. Holder (2017), Light-absorbing organic carbon from prescribed  
1457 and laboratory biomass burning and gasoline vehicle emissions. *Scientific Reports*, 7, 7318.  
1458  
1459 Verma, S., and Coauthors (2009), Ozone production in boreal fire smoke plumes using  
1460 observations from the Tropospheric Emission Spectrometer and the Ozone Monitoring  
1461 Instrument. *J. Geophys. Res.*, 114, D02303.  
1462  
1463 Viegas, D. X. (1998), Convective processes in forest fires, in: Buoyant  
1464 Convection in Geophysical Flows, edited by: Plate, E. J., Fedorovich, E. E., Viegas, D. X., and  
1465 Wyngaard, J. C., Kluwer Academic Publishers, AA Dordrecht, The Netherlands, pp. 401–420  
1466  
1467 Yokelson, R., D. Griffith, and D. Ward (1996), Open-path Fourier transform infrared studies of  
1468 large-scale laboratory biomass fires. *J. Geophys. Res.-Atmos.*, 101, 21067–21080.  
1469  
1470 Zaveri, R. A., R. C. Easter, J. D. Fast, and L. K. Peters (2008), Model for simulating aerosol  
1471 interactions and chemistry (MOSAIC), *J. Geophys. Res.*, 113, D13204.  
1472  
1473 Zhang, L. M., S. L. Gong, J. Padro, L. Barrie (2001), A size-segregated particle dry deposition  
1474 scheme for an atmospheric aerosol module. *Atmos. Environ.*, 35, 549–560.  
1475  
1476 Zhang, Y., J. Fan, T. Logan, Z. Li, and C. R. Homeyer (2019), Wildfire impact on environmental  
1477 thermodynamics and severe convective storms. *Geophys. Res. Lett.*, 46, 10082–10093.  
1478  
1479 Zou, Y. and Coauthors (2019). Machine learning-based integration of high-resolution wildfire  
1480 smoke simulations and observations for regional health impact assessment. *J. Environ. Res.*  
1481 *Public Health*, 16, 2137.  
1482  
1483